Molecular Therapy
Nucleic Acids
Original Article

Preclinical characterization of antagomiR-218 as a potential treatment for myotonic dystrophy

Estefanía Cerro-Herreros,[1,2] Irene González-Martínez,[1,2] Nerea Moreno,[1,2] Jorge Espinosa-Espinosa,[1,2] Juan M. Fernández-Costa,[1,2,10] Anna Colom-Rodrigo,[1,2] Sarah J. Overby,[1,2] David Seoane-Miraz,[7,8] Javier Poyatos-García,[3,4,5] Juan J. Vilchez,[3,4,5] Adolfo López de Munain,[6,9] Miguel A. Varela,[7,8] Matthew J. Wood,[7,8] Manuel Pérez-Alonso,[1,2] Beatriz Llamusí,[1,2,11] and Rubén Artero[1,2]

[1]University Research Institute for Biotechnology and Biomedicine (BIOTECMED), Universidad de Valencia, Dr. Moliner, 50, 46100 Burjasot, Valencia, Spain; [2]Incliva Biomedical Research Institute, Avenida Menéndez Pelayo 4 acc, 46010 Valencia, Spain; [3]The IISLAFE Health Research Institute, Avenida Fernando Abril Martorell, 106 Torre A 7ª planta, 46026 Valencia, Spain; [4]Neuromuscular Reference Centre ERN EURO-NMD and Neuromuscular Pathology and Ataxia Research Group, Hospital La Fe Health Research Institute, Valencia, Spain; [5]Centro de Investigación Biomédica en Red de Enfermedades Raras (CIBERER), Instituto de Salud Carlos III, Madrid, Spain; [6]Biodonostia Health Research Institute, P° Dr. Beguiristain s/n, 20014 Donostia–San Sebastián, Spain; [7]Department of Paediatrics, University of Oxford, John Radcliffe Hospital, Headley Way, OX3 9DU, Oxford, UK; [8]MDUK Oxford Neuromuscular Centre, University of Oxford, Oxford, UK; [9]Hospital Universitario Donostia-Osakidetza-Departamento de Neurociencias-Universidad del Pais Vasco-CIBERNED

Myotonic dystrophy type 1 (DM1) is a rare neuromuscular disease caused by expansion of unstable CTG repeats in a non-coding region of the *DMPK* gene. CUG expansions in mutant *DMPK* transcripts sequester MBNL1 proteins in ribonuclear foci. Depletion of this protein is a primary contributor to disease symptoms such as muscle weakness and atrophy and myotonia, yet upregulation of endogenous MBNL1 levels may compensate for this sequestration. Having previously demonstrated that antisense oligonucleotides against miR-218 boost MBNL1 expression and rescue phenotypes in disease models, here we provide preclinical characterization of an antagomiR-218 molecule using the HSA^{LR} mouse model and patient-derived myotubes. In HSA^{LR}, antagomiR-218 reached 40–60 pM 2 weeks after injection, rescued molecular and functional phenotypes in a dose- and time-dependent manner, and showed a good toxicity profile after a single subcutaneous administration. In muscle tissue, antagomiR rescued the normal subcellular distribution of Mbnl1 and did not alter the proportion of myonuclei containing CUG foci. In patient-derived cells, antagomiR-218 improved defective fusion and differentiation and rescued up to 34% of the gene expression alterations found in the transcriptome of patient cells. Importantly, miR-218 was found to be upregulated in DM1 muscle biopsies, pinpointing this microRNA (miRNA) as a relevant therapeutic target.

INTRODUCTION

In contrast to most genetic diseases, which stem from lack of a protein function due to a mutation in the encoding gene, myotonic dystrophy type 1 (DM1) originates from the depletion of Muscleblind-like 1 (MBNL1) and 2 (MBNL2) proteins due to sequestration by toxic RNAs forming microscopically visible ribonuclear structures known as foci.[1,2] This is favorable for therapy, since protein depletion can be compensated by degradation of toxic RNA[3,4] or enhanced expression of genes encoding the depleted proteins,[5,6] which remain perfectly functional in patients, in an approach termed therapeutic gene modulation. DM1 is a rare autosomal dominant neuromuscular disease that is characteristically multisystemic, with highly variable clinical phenotypes encompassing the central nervous system (CNS), heart, and skeletal and visceral musculature.[7] Skeletal muscle alterations include myotonia and muscle weakness and atrophy, which contribute significantly to disease morbidity and mortality due to respiratory distress, dysphagia, and immobility.[8] The mutation causing DM1 is an expansion in the number of CTG trinucleotide repeats in the 3′ untranslated region (UTR) of *DM1 protein kinase* (*DMPK*[9,10]). Above ∼50 repeats, they become transcribed into mutant *DMPK* transcripts; these fold into CUG RNA hairpins that sequester MBNL1 and 2 proteins. This gives rise to molecular defects and phenotypes similar to loss of MBNL1 and 2 functions, as demonstrated in mice by knockout of *Mbnl1*[11] or *Mbnl2*[12] or the compound loss of both.[13] This hypothesis is further supported by experiments in which phenotypes produced by targeted expression of CUG repeats expanded in the skeletal muscles driven by human skeletal actin transgene (HSA^{LR}[14]) are rescued by adeno-associated virus-[15] or transgene-mediated overexpression of Mbnl1,[16] and also by candidate drugs that rescue disease-like phenotypes through upregulation

Received 18 October 2020; accepted 17 July 2021;
https://doi.org/10.1016/j.omtn.2021.07.017.

[10]Present address: Institute for Bioengineering of Catalonia, The Barcelona Institute of Science and Technology (BIST), Calle Baldiri Reixac 10-12, 08028 Barcelona, Spain

[11]Present address: Arthex Biotech, Calle Catedrático Agustín Escardino Benlloch, 9, 46980 Paterna, Valencia, Spain

Correspondence: Rubén Artero, Translational Genomics Group. University Research Institute for Biotechnology and Biomedicine (BIOTECMED), Universidad de Valencia, Dr. Moliner, 50, 46100 Burjasot, Valencia, Spain.
E-mail: ruben.artero@uv.es

of *MBNL1* gene expression in human cells and mouse and *Drosophila* models.[5,6,17,18–20] *Mbnl1* loss of function also accounts for >80% of mis-splicing events and nearly 70% of expression defects in the HSA^{LR} mouse model.[21,22] MBNL1 also reverses the proliferation defects of skeletal muscle satellite cells in DM1.[23]

MBNL proteins are master switches in fetal-to-adult splicing transition[22,24] and polyadenylation[25] in the skeletal muscles but are also known to participate in regulated biogenesis of microRNAs (miRNAs),[26] mRNA stability,[27] translation and protein secretion,[28] and subcellular localization of transcripts.[29] MBNL1 plays a primary role in controlling alternative splicing in skeletal and cardiac muscle, and MBNL2 serves a related function in the CNS.[12] Genetic redundancy is well illustrated by the fact that deletion of only one paralog resulted in the upregulation of the other and occupancy of its binding sites.[13] Whereas MBNL proteins promote adult-type alternative splicing patterns, CUGBP Elav-like family member 1 (CELF1), which is abnormally activated in skeletal muscle in DM1, promotes the fetal type,[30] as similarly described also for heterogeneous nuclear ribonucleoprotein A1 (hnRNPA1).[31] Maintaining a fetal alternative splicing pattern in muscle transcripts in adults results in unfit proteins that cause specific symptoms, as demonstrated by *chloride voltage-gated channel 1* (*CLCN1*[32]) or *bridging integrator 1* (*BIN1*[33]) transcripts. Genome-wide alterations in the transcriptome of patients have recently been reported in detail.[34]

We have previously demonstrated that hsa-miR-218-5p (hereafter miR-218) is a natural *MBNL1* and *2* repressor in human myotubes and mice and that its inactivation through antisense oligonucleotide (antagomiR)-mediated blocking leads to miRNA depletion and MBNL1 and 2 protein upregulation.[19] Here we expand on these observations by addressing the dose response, duration, and toxicity of antagomiR-218 treatments as well as characterizing their effect at the transcriptome level and biodistribution. We also report that miR-218 is significantly overexpressed in DM1 muscle samples and disease models, thus potentially contributing to disease phenotypes through MBNL1- and 2-independent pathways. These results underline the therapeutic potential of miR-218 blocking oligonucleotides as potential treatments for DM1.

RESULTS

MBNL1 is a direct target of miR-218

We previously showed that miR-218 directly regulated *MBNL2* stability and expression through 3′ UTR luciferase sensor constructs, but the potential regulation of human or mouse *MBNL1* was not formally addressed.[19] Specifically, in mice, according to the bioinformatics tools miRDB, miRanda, and TargetScan, there are four predicted target sites for miR-218, whereas in humans only two are conserved (Figures S1A and S1B). When combining miR-218 with mouse *Mbnl1* 3′ UTR wild-type sensor constructs in C2C12 cells, a decrease in luciferase is observed, but when using the versions with the mutated target sites, only the one with the mutation in site 3 stops responding. Thus, the active repressor site for miR-218 is number 3 (Figure 1A). Consistently, perfect-match (PM) constructs for all four candidate sites confirm a decrease in luciferase and verify that the plasmid is expressing miR-218. Finally, in HeLa cells, we confirmed the functional conservation of mouse miR-218 site 3 in human *MBNL1* 3′ UTR sensor constructs, using a synthetic agomiR-218 (Figure S1C).

Using a similar approach, we transfected HeLa cells with a luciferase 3′ UTR *MBNL1* fusion construct containing the wild-type predicted binding sites for miR-218 according to miRecords[35] (Figure S1C). A preexisting construct containing a perfect match for miR-218 in the *MBNL2* 3′ UTR served as a positive control. Co-transfection of reporter constructs and a synthetic miR-218 agomiR demonstrated a robust reduction of *Gaussia* luciferase expression, whereas a negative control agomiR with a scramble sequence (SC) failed to repress the construct (Figure S1C). Thus, these results demonstrate the direct recognition of at least one miR-218 binding site in the *MBNL1* 3′ UTR.

Similar antagomiR-218 efficacy via subcutaneous and intravenous administration

To account for potential differential effects depending on the administration route, we tested the activity of 12.5 mg/kg of antagomiR-218 by subcutaneous and intravenous injection in HSA^{LR} model mice, which we have used previously in similar analyses and are readily available in our premises. Four days post injection, gastrocnemius and quadriceps muscles were processed to quantify miR-218, and *Mbnl1* at the RNA and protein levels (Figures S2A–S2E). miR-218 levels were under 50% of normal amounts, and *Mbnl1* transcripts and proteins were upregulated, yet differences between subcutaneous and intravenous administration were negligible in both muscles except for *Mbnl1* transcripts in quadriceps. Both administration types rescued weight-normalized grip strength, but intravenous delivery yielded significantly greater rescue than subcutaneous delivery, whereas myotonia was only rescued when antagomiR-218 was subcutaneously provided (Figures S2F and S2G). Taking these results together, we detected no difference in miRNA and Mbnl1 protein levels, whereas functional rescues were more consistent with subcutaneous delivery. Several parameters were analyzed in total blood obtained before sacrifice to check whether administration routes differentially altered blood biochemistry. These parameters showed more alterations in intravenous administrations than subcutaneous treatment and normalized to PBS (Table S1, Tab A). Amylase and total bilirubin were significantly increased compared with mice injected subcutaneously with antagomiR-218. The scramble (SC) negative control also showed alterations in lipase after intravenous injection. However, the levels achieved were reported as not clinically relevant.[36] Unaltered weight and visual necropsy confirmed no major toxic effects in the treated mice. Analysis of the white blood cell differential count from mice treated with antagomiR-218 via the two administration routes found no significant differences, with a similar conclusion in mice treated with SC (Table S1, Tab B). These results confirm that both administration routes are effective as therapy. However, the ability to compare with previous studies together with the experimental ease of subcutaneous injections prompted us to use this delivery method in all subsequent experiments.

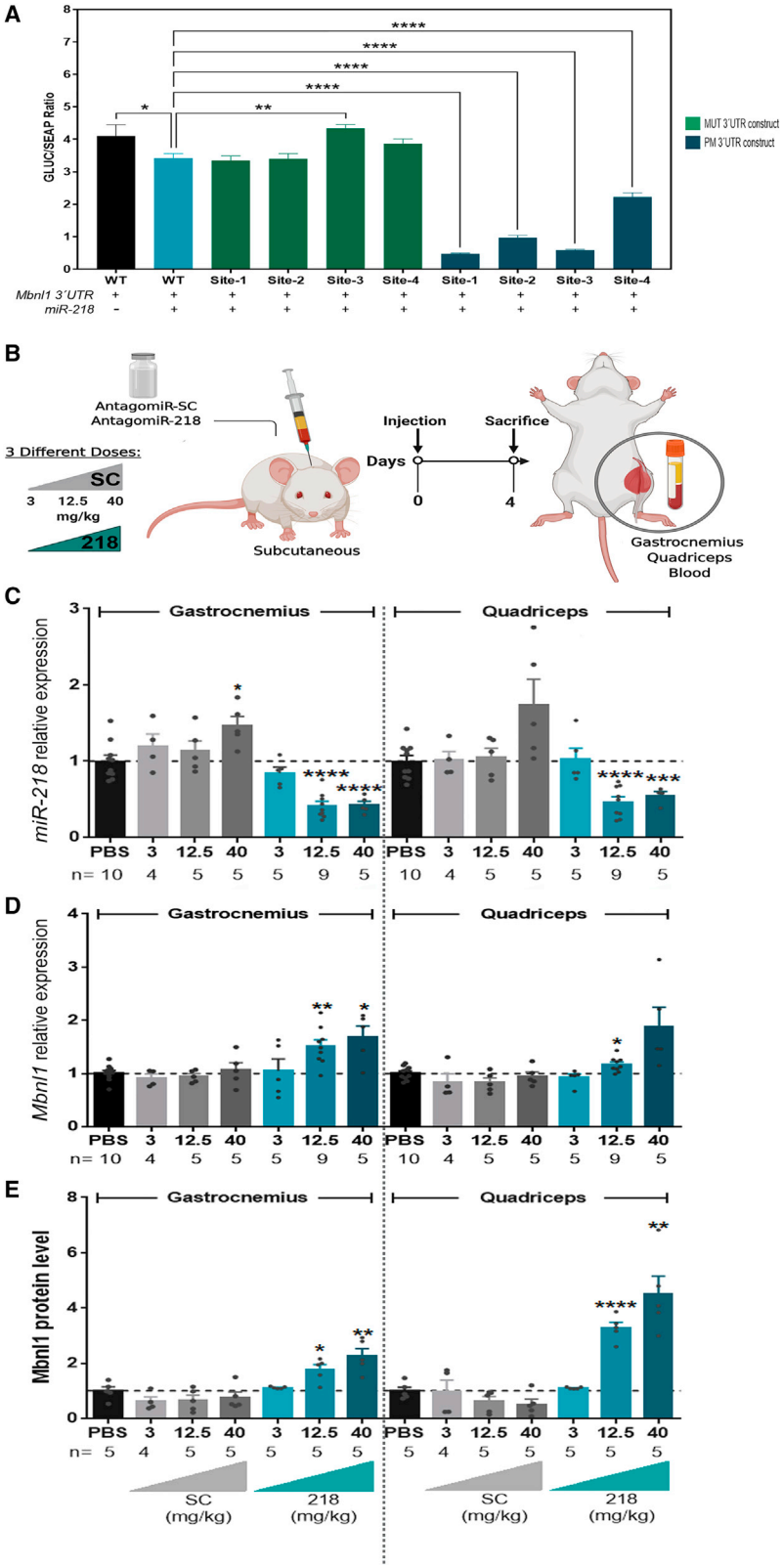

Figure 1. Expression levels of direct molecular targets correlate appropriately with varying antagomiR-218 doses

(A) *Gaussia* luciferase levels, relative to internal control secreted alkaline phosphatase (SEAP), are shown for C2C12 cells co-transfected with mouse *Mbnl1* 3′ UTR reporter constructs (wild-type [WT], mutated [MUT], and perfect match [PM]) and pVmiR-218 (abbreviated miR-218). (B) Experimental design of the dose-response study to test three concentrations (3, 12.5, and 40 mg/kg) by subcutaneous administration. (C–E) Gastrocnemius and quadriceps muscles were dissected 4 days post injection to detect miR-218 expression relative to U1 and U6 snRNA endogenous controls (C) (levels may be overestimated in the 40 mg/kg condition because amplification occurred at cycle threshold close to 35 cycles and amplification actually failed in some samples); *Mbnl1* transcript expression relative to *Gapdh* endogenous control (D); and Mbnl1 protein levels (E) by ELISA and normalized to total protein. N indicates the number of mice used in each experiment. Statistical comparisons were all performed against PBS-treated HSA^{LR} values (indicated by a black dashed line) with a Student's t test. *$p < 0.05$, **$p < 0.01$, ***$p < 0.001$.

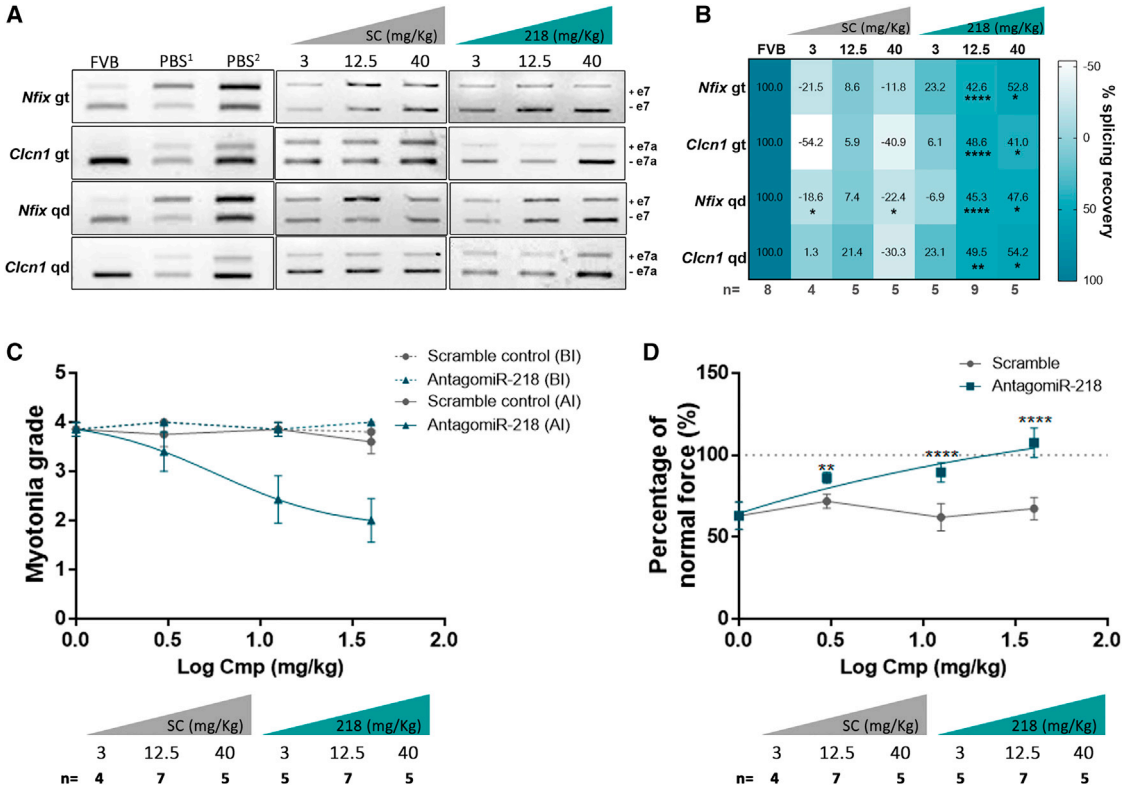

Figure 2. Subcutaneous antagomiR-218 improved mis-splicing of Mbnl-dependent transcripts, myotonia, and force in a dose-dependent fashion in HSA^{LR} mice

(A) RT-PCR analyses of the splicing of *Nfix* exon 7 and *Clcn1* exon 7a in gastrocnemius (gt) and quadriceps (qd) muscles. PBS1 control corresponds to 12.5 mg/kg treatment, and PBS2 corresponds to 3 and 40 mg/kg treatments. Exon inclusion levels of healthy control mice are shown for FVB. Quantification of these representative exon inclusion results is provided in Figure S4. (B) Heatmap representing the percentage of normal splicing recovery for *Nfix* and *Clcn1* in gt and qd in treated HSA^{LR} mice according to the color scale provided. (C and D) Myotonia grade (C) and percentage of normal grip strength (D) were analyzed before injection (BI) and 4 days after injection (AI). N indicates the number of mice used for each experiment. Each treatment was statistically compared with its respective PBS control via Student's t test. *p < 0.05, **p < 0.01, ***p < 0.001.

The effects of antagomiR-218 depend on the dosage

AntagomiR-218 was previously tested at a single dose of 12.5 mg/kg,[19] but this failed to confirm that its molecular and *in vivo* effects depended on the concentration of the oligonucleotide, or whether this response was linear or otherwise. To this end, we subcutaneously injected antagomiR-218 at a low (3 mg/kg), intermediate (12.5 mg/kg), or high (40 mg/kg) concentration and recovered quadriceps and gastrocnemius muscles (Figures 1B–1E). miR-218 levels were not significantly different from normal at 3 mg/kg, but both intermediate and high concentrations similarly lowered miR-218 to slightly below 50% of normal levels. Of note, the SC negative control nonspecifically increased miR-218 levels at the highest concentration. In contrast to the plateau detected for miR-218 levels at 12.5 and 40 mg/kg, Mbnl1 transcripts and protein amount increased steadily with dose in both muscles, although the statistical differences were more or less significant depending on the magnitude of the error. In general, 3 mg/kg was too low to significantly enhance Mbnl1 expression at the transcript or protein level, except in quadriceps, which exhibited the most robust response in terms of Mbnl1 protein amounts, and both muscles showed a similar pattern of response to antagomiR-218 administrations. Importantly, treatment did not significantly alter *HSA* transgene expression (Figure S3A). Thus, two direct molecular readouts of antagomiR-218 activity (Mbnl1 mRNA and protein levels) respond to the antagomiR dose in an approximately linear fashion (Figures S3B–S3E), whereas miR-218 levels seem to plateau at the highest concentration tested. Nevertheless, miRNA levels get further reduced if compared to negative control SC, which unspecifically increases miR-218 levels (Figure S3F).

Enhanced expression of Mbnl1 in HSA^{LR} model mice was confirmed to rescue characteristic exon inclusion events, myotonia, and grip strength in a dose-dependent manner (Figure 2; Figure S4). *Nfix* and *Clcn1* transcripts showed abnormally increased inclusion of exon 7 in HSA^{LR} mice, but this recovered to ~40%–50% of normal values at 12.5 mg/kg in muscles. The low dose was unable to significantly improve mis-splicing, whereas the high dose only marginally enhanced exon inclusion rescue compared with the intermediate dose values. Turning to functional measurements, myotonia grade was 4 for DM1 mice and progressively dropped to almost 2 (myotonic discharges at only half of the electrode insertions) at the highest dose

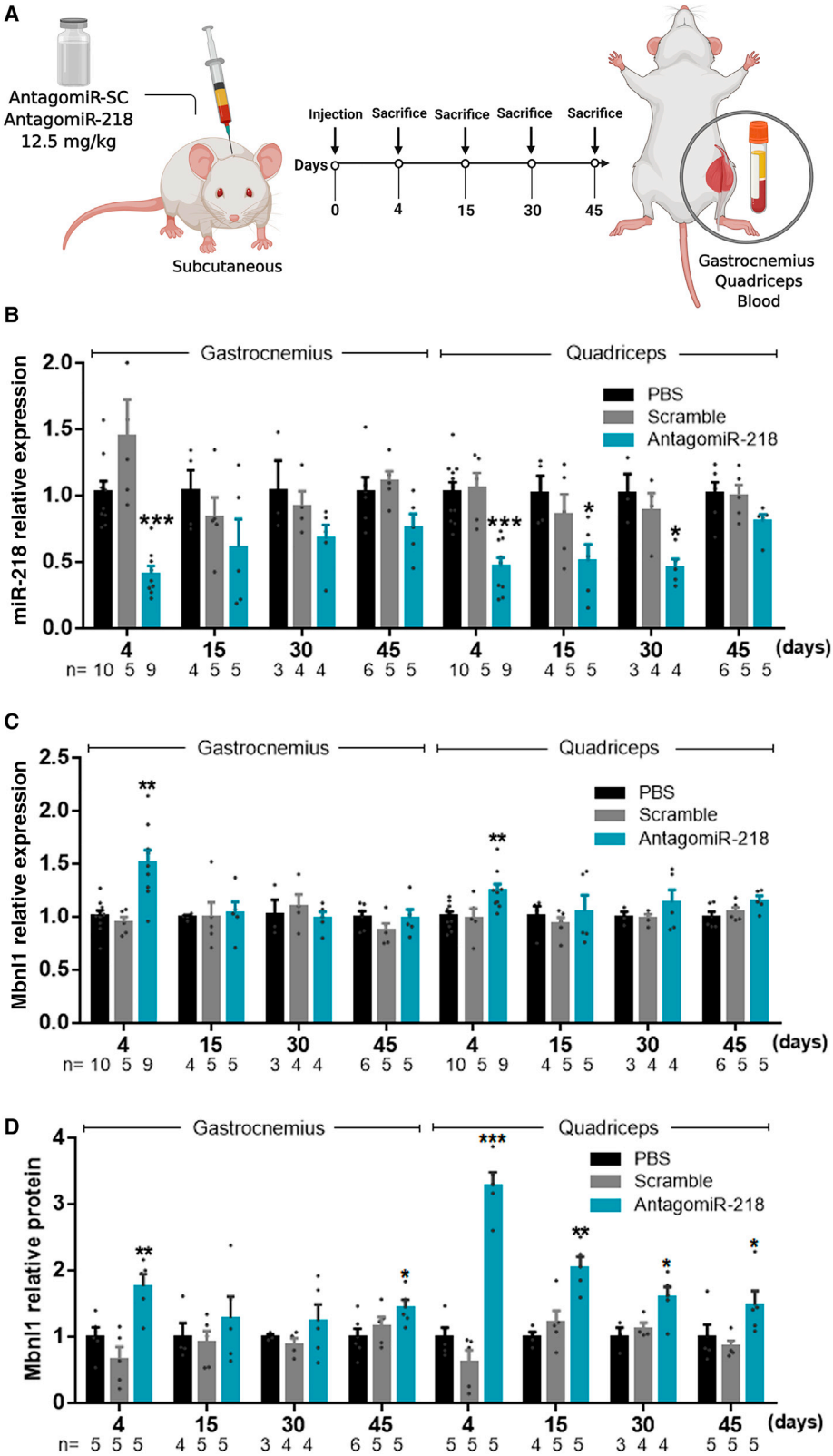

(legend on next page)

tested. Weight-normalized grip strength was ~70% of normal in control-treated HSA^{LR} mice but significantly improved at all concentrations tested and reached close to normal values at intermediate and high doses. In summary, antagomiR-218 was shown to rescue the characteristic mis-splicing defects described in the model mice and improved myotonia and grip strength in a dose-dependent manner, but with a trend toward a plateau effect at 40 mg/kg.

Different biochemical parameters were analyzed in total blood obtained before sacrifice to check for potential deleterious effects in response to increasing doses. Neither antagomiR-SC nor antagomiR-218 treatments caused significant alterations in quantified tissue damage biomarkers compared with PBS (Table S1, Tab C). Mouse weight also showed no significant changes between the different treatments, and visual necropsies were normal at all dosages tested. Nevertheless, ANOVA and Kruskal-Wallis analyses revealed statistically significant differences in urea levels and body weight between Friend Virus B (FVB) and HSA^{LR} mice treated with PBS, and lipase levels were also significantly different between FVB and HSA^{LR} mice treated with PBS, SC, and antagomiR-218. Therefore, these alterations seem more closely associated with disease state than experimental treatment, consistent with previous reports.[37] Analyzing white blood cell differential count, there were no significant treatment- or dose-related differences between the groups analyzed (note the lack of clustering among treated mice in the dendrogram of Table S1, Tab D). Overall, these data support that even the highest concentration tested caused no significant modification of blood biochemistry parameters.

One single injection of antagomiR-218 produces weeks-lasting molecular and phenotypic improvements

Our previous description of antagomiR-218 activity was at 4 days,[19] but a similar antagomiR was recently reported to bring about functional recoveries lasting up to 45 days in the HSA^{LR} mouse model.[37] To test whether the same was true for antagomiR-218, we subcutaneously injected 12.5 mg/kg of product and sacrificed animals at 4, 15, 30, and 45 days post injection (Figure 3A), also using this experiment to test for potential long-term toxic effects. Data analysis revealed differential effects depending on the muscle studied (Figures 3B–3D), with more lasting molecular consequences in quadriceps than gastrocnemius. In particular, miR-218 reduction and Mbnl1 protein increase in quadriceps were significant up to 30 and 45 days post injection, respectively, whereas the increase in *Mbnl1* transcripts was only statistically robust for 4 days after administration. In gastrocnemius, in contrast, antagomiR-218-induced changes in miRNA and *Mbnl1* transcripts and protein were only clearly significant at day 4, whereas Mbnl1 protein levels were statistically significant at day 45 but did not differ meaningfully from protein assessment of the same muscle at days 15 and 30. Therefore, experimental treatment duration is muscle dependent, with more lasting effects in the quadriceps muscle than in gastrocnemius. At 45 days after a single subcutaneous injection of antagomiR-218, Mbnl1 protein levels were still significantly upregulated in quadriceps muscles compared with SC- or PBS-treated conditions.

The functional relevance of the molecular rescues triggered by antagomiR-218 over time was also assessed at the alternative splicing level, in myotonia and grip strength (Figure 4; Figure S5). Aberrant inclusion of exon 7 of *Nfix* and 7a of *Clcn1* was assessed as before, but from gastrocnemius and quadriceps samples of HSA^{LR} mice several days after administration of the experimental treatment or a negative (SC) or procedural (PBS) control. In short, alternative splicing rescues were only significant for both *Nfix* and *Clcn1* at 4 and 15 days post injection in quadriceps, in concordance with the robust upregulation of Mbnl1 in this muscle, whereas in gastrocnemius only rescue of *Clcn1* splicing was significant at both time points. Force recovery followed a similar pattern, and the percentage of normal force was significantly higher in treated mice up to 15 days post injection, despite values staying around 100% of normal mouse grip strength up to experiment completion on day 45. Reduction of myotonia grade was weak after day 4 but sustained over time. Collectively, these results indicate that molecular rescues do not extend beyond 4 days post injection in the gastrocnemius muscle but in quadriceps can last up to 45 days and correlate with weeks-lasting functional improvements in terms of grip strength and myotonia.

The biochemistry parameters from whole blood obtained before sacrifice showed that neither antagomiR-SC nor antagomiR-218 treatments caused significant alterations in organ damage biomarkers or visual necropsy at the different time points compared with PBS treatment (Table S1, Tab E). There was, however, a significant difference between FVB and PBS in body weight and amylase levels, although values were similar in comparisons between antagomiR-218-treated and FVB and between antagomiR-218-treated and PBS-injected HSA^{LR} control mice. As for the white blood differential count, there were no significant differences between any of the groups, implying no changes in blood composition associated with treatment or time, as illustrated by the lack of any significant clustering in the dendrogram shown in Table S1, Tab F.

AntagomiR-218 reaches the muscles and rescues normal Mbnl1 distribution *in vivo* with no change in the proportion of myonuclei with microscopically visible foci

An essential parameter to assess the therapeutic potential of antagomiR-218 is how much oligonucleotide reaches the different tissues

Figure 3. Duration of antagomiR-218 therapeutic effects upon single subcutaneous injection

(A) Experimental design after a single subcutaneous injection of 12.5 mg/kg antagomiR-218. Mice were sacrificed 4, 15, 30, and 45 days post injection, quadriceps and gastrocnemius muscles were dissected, and blood was collected. (B–D) Relative expression of miR-218 (B), *Mbnl1* transcripts (C), and Mbnl1 protein (D) from gastrocnemius and quadriceps muscles relative to U1 and U6 snRNA, *Gapdh*, and total protein, respectively. miR-218 and transcripts were quantified by qRT-PCR, and protein levels were determined by ELISA. N indicates the number of mice used for the experiment. All statistical comparisons were performed against the data obtained in PBS-treated HSA^{LR} mice (black dashed line) with Student's t test. *$p < 0.05$, **$p < 0.01$.

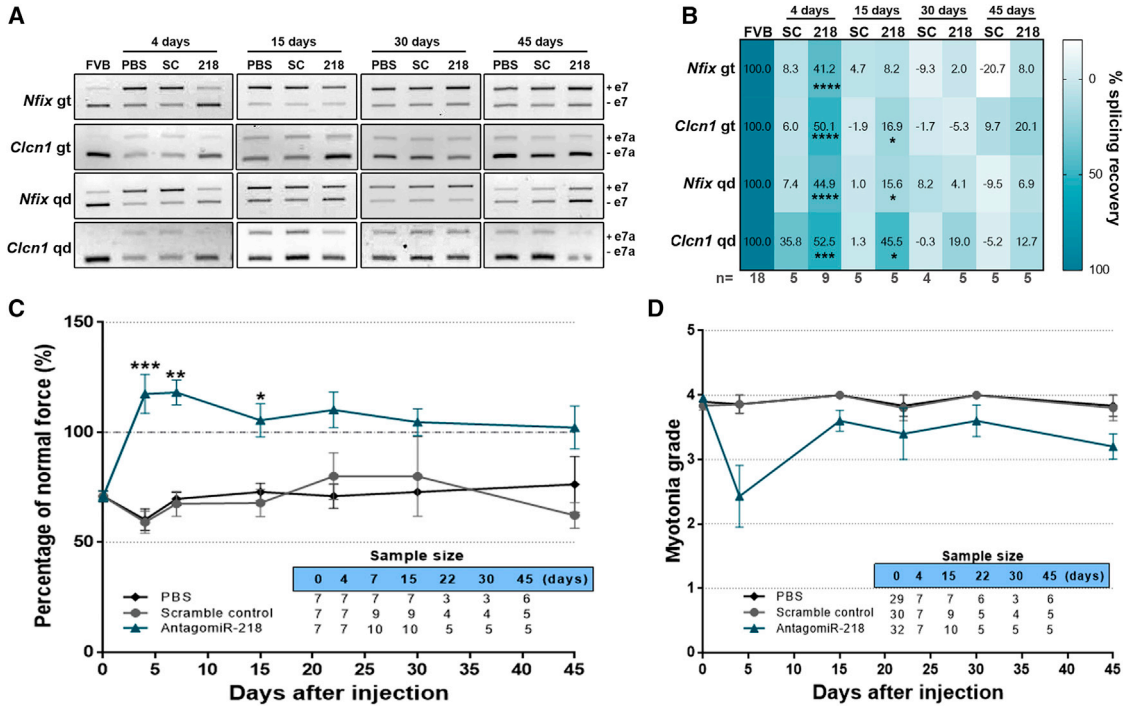

Figure 4. Subcutaneous antagomiR-218 improved mis-splicing of Mbnl-dependent transcripts, myotonia, and force in a time-dependent fashion in HSA^{LR} mice

(A) Representative images of RT-PCR gels to quantify *Nfix* exon 7 and *Clcn1* exon 7a inclusion in gastrocnemius (gt) and quadriceps (qd) muscles at the indicated days post treatment with PBS, SC, or antagomiR-218. Quantification of the individual exon inclusion percentages is provided in Figure S5. (B) Heatmap representing the percentage of exon inclusion recovery calculated for *Nfix* and *Clcn1* in gt and qd of HSA^{LR} mice upon indicated experimental conditions. The percentage of exon inclusion recovery was calculated as in Figure 2. (C) Percentage of normal grip strength (normalized to weight) were analyzed before injection, at the indicated intermediate time points, and before the sacrifice and (D) Myotonia. N indicates the number of mice used for each experiment. For statistical analyses, each experimental condition was compared to the corresponding PBS control with a Student's t test. *$p < 0.05$, **$p < 0.01$, ***$p < 0.001$.

and organs *in vivo* upon systemic delivery. To this end, a custom ELISA method was employed to detect the molecule in tissue homogenates of gastrocnemius, quadriceps, brain, heart, kidney, and liver (Figure 5A) 2 weeks after a single subcutaneous injection. Furthermore, a Cy3-labeled antagomiR-218 was injected subcutaneously into one mouse, and its accumulation to kidney and liver, as previously described for other oligonucleotides with similar chemistries,[38] was evident by direct visualization under the fluorescence microscope (Figures S6A and S6B). Besides liver and kidney, the antagomiR-218 was highly detected in the heart (~10 nM), whereas the concentration in skeletal muscles ranged between 40 and 60 pM and in the brain was almost indetectable.

Next, we hypothesized that *in vivo* enhanced amounts of Mbnl1 protein could freely diffuse within muscle fibers or promote additional protein sequestration by ribonuclear CUG foci. To test these possibilities, we performed immunofluorescence analysis of Mbnl1 levels and subcellular distribution in quadriceps muscle sections and quantification of foci in the same muscle (Figure 5). Quantification of immunofluorescence signals detected a significant increase in Mbnl1 levels in the quadriceps of HSA^{LR} mice treated with 12.5 mg/kg of antagomiR-218 compared to negative (SC) or procedure (PBS) controls (Figures 5B and 5D–5G). The signal not only was higher in antagomiR-218-treated muscles than controls but also showed a subcellular distribution closely resembling normal muscles, in features such as dispersed signal through the cytoplasm and the cell nucleus. The proportion of myonuclei with expanded CUG foci was unchanged by antagomiR-218 in mouse quadriceps compared to controls and was similar to previous findings,[39] which strongly reinforces previous observations that extra Mbnl1 is not further sequestered by CUG repeat expansions but rather compensates for preexisting depletion of Mbnl1 proteins.[19,37] The impact of antagomiR-218 in the brain and heart mouse samples was assessed at the miRNA (miR-218) and transcript and protein levels (Mbnl1; Figures S6C–S6E). Interestingly, miR-218 lowered to about half normal levels in antagomiR-treated mice, which correlated with significant increases in Mbnl1 at the transcript and protein levels. Although we do not discard a direct effect by the antagomiR itself, since it can be detected in brain samples in minute amounts (Figure 5A), we suggest potential non-autonomous effects mediated by myokines or energy metabolism regulators, among other possibilities. miR-218 was not detected in the mouse[40] and human[41]

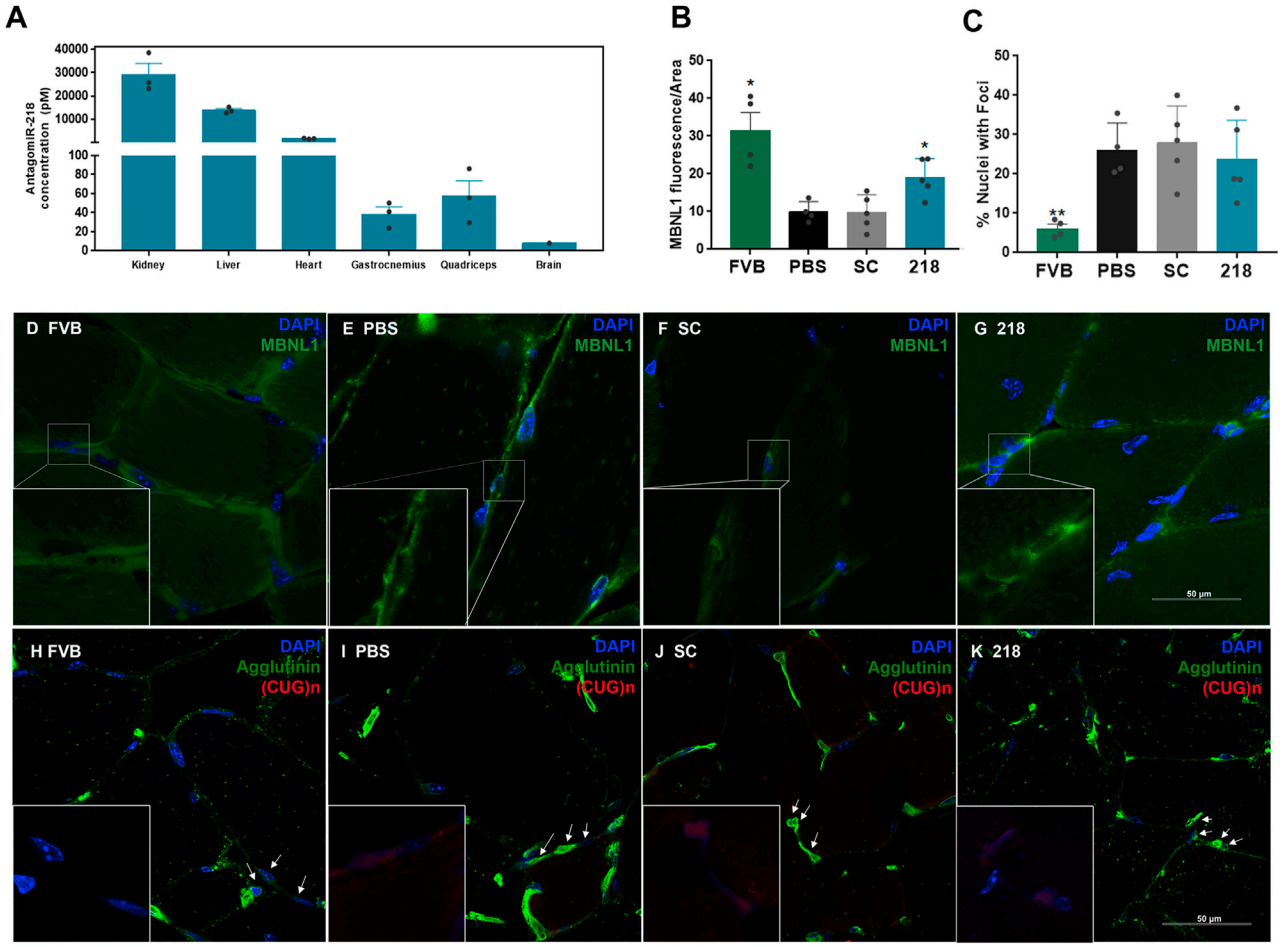

Figure 5. AntagomiR-218-mediated upregulation of Mbnl1 is not additionally sequestered in ribonuclear foci in HSA^{LR} mouse muscles

(A) Biodistribution of antagomiR-218 reveals effective delivery to cardiac tissue after subcutaneous systemic injection in DM1 mice. Two weeks after subcutaneous systemic injection in HSA^{LR} mice (n = 3), antagomiR-218 concentration was low in the brain (only detectable in one of the mice) and modest in skeletal muscle (25–100 pM), whereas the concentration in cardiac muscle was more than one order of magnitude higher (1.6 nM). AntagomiR-218 concentration was detected by a custom ELISA assay using probes labeled with digoxigenin and biotin (error bars, SEM). (B and C) 12.5 mg/kg of antagomiR-218 or negative control (SC) or vehicle-only (PBS) was subcutaneously administered to HSA^{LR} mice. PBS-treated FVB was the healthy control. Four days post injection, quadriceps muscles were processed for immunofluorescence (IF) or fluorescence *in situ* hybridization (FISH). (B) Quantitation of Mbnl1 signal from tissue sections processed for IF. (C) Quantitation of the percentage of muscle nuclei with at least one foci from FISH processed muscle sections. (D–G) Representative confocal images of Mbnl1 (green) staining in healthy mice (FVB) and HSA^{LR} mice after subcutaneous injection with antagomiR-218, antagomiR-SC, and PBS. Nuclei were counterstained with DAPI (blue). In HSA^{LR} quadriceps, endogenous Mbnl1 was in nuclear aggregates (green puncta) and the total amount of protein was reduced compared with FVB muscles (D and E). In contrast, HSA^{LR} quadriceps muscle treated with antagomiR-218 showed a robust increase in cytoplasmic and nuclear Mbnl1 levels in the fibers (G) compared with control-treated HSA^{LR} (antagomiR-SC) (F) and vehicle only (PBS) (E). (H–K) Representative FISH images showing (CUG)n RNA foci (red) performed with cryosections from the quadriceps of control FVB (H) and HSA^{LR} mice treated with antagomiR-218 (K), antagomiR-SC (J), and PBS (I). Wheat germ agglutinin staining (green) was used to highlight individual myofibers, and nuclei were counterstained with DAPI (blue). Arrows point to the nuclei shown in the inset. For Mbnl1 IF and foci quantification, a total of 8 images (at 400× magnification) from each mouse muscle were analyzed: n = 4 for FVB, PBS, and antagomiR-218; n = 5 for antagomiR-SC. Scale bars, 50 µm. All cryosections were 10 µm thick, and images were compiled from multiple projections in Z-plane stacks. All images were acquired under the same settings. *$p < 0.05$, **$p < 0.01$, ***$p < 0.001$.

liver. Therefore, despite it accumulating in this organ, these observations argue against the possibility of adverse effects resulting from the reduction in miR-218 levels. Furthermore, we have collected available information from public databases to generate Figure S6F, which summarizes quantitative PCR data from the indicated human tissues and organs reported by miRNAMap.[41]

miR-218 is overexpressed in DM1 disease models and patient muscle biopsies

Silencing of miR-218 by therapeutic antisense oligonucleotides has the potential drawback of generating loss-of-function phenotypes should miRNA maintain normal, or reduced, expression levels in DM1 muscle. To specifically test this hypothesis, we determined miR-218 amounts by

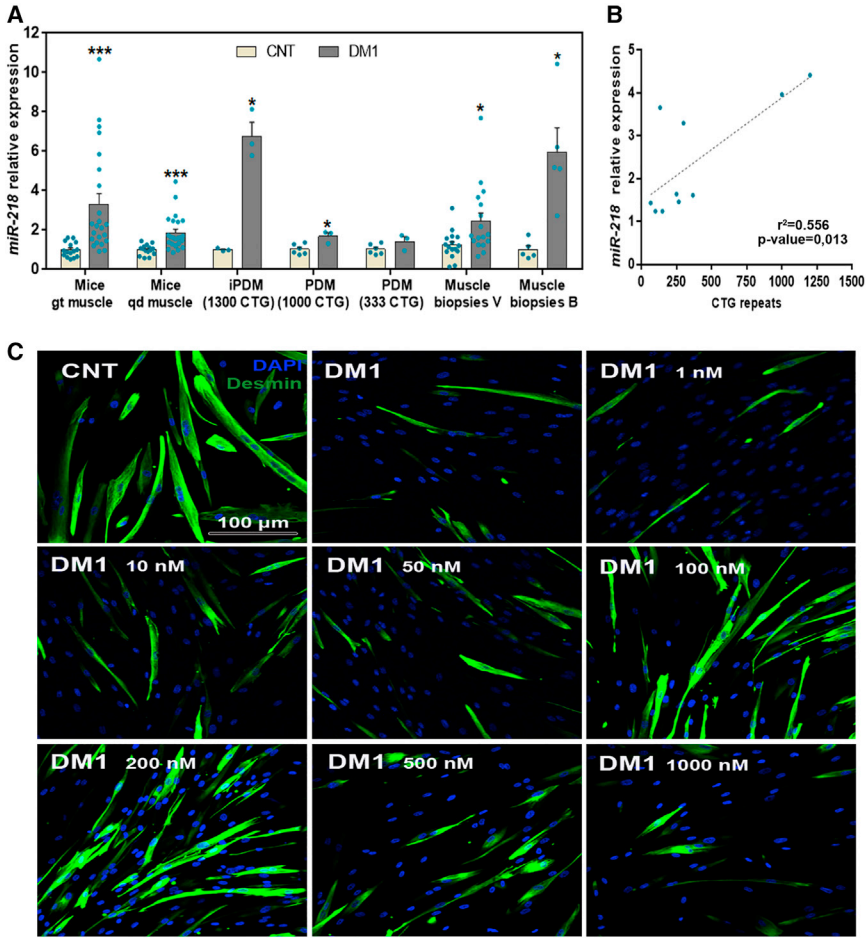

Figure 6. miR-218 is overexpressed in several DM1 disease models and patient muscle biopsies

(A) Quantification by qRT-PCR of the relative expression of miR-218 in gastrocnemius and quadriceps of HSA^{LR} and FVB mice, in control and immortalized DM1 (iPDM[42]) and non-immortalized (PDM) myotubes, derived from patients with the indicated number of CTG repeats, and muscle biopsies of patients and controls. V indicates the cohort from Hospital La Fe (Valencia, Spain), and B indicates a cohort from the Biodonostia Institute (San Sebastian, Spain). Quantification is normalized to the mean expression of the corresponding control groups. The endogenous reference genes were snRNA U1 and U6, in addition to miR-103 in the case of both iPDM and PDM myotubes. Individual data points are indicated. (B) miR-218 levels positively correlated with the expansion size for a comparable subset of human biopsies from the deltoid muscles of the Valencia patient cohort. (C) Representative confocal images of healthy control (CNT) and DM1 cells treated for 4 days with the indicated amounts of antagomiR-218 and immunostained for Desmin (green) and contrasted with DAPI (blue) to mark the nucleus. Scale bars, 100 µm. *$p < 0.05$, **$p < 0.01$, ***$p < 0.001$.

quantitative reverse transcriptase PCR (qRT-PCR) in skeletal muscles (gastrocnemius and quadriceps) from HSA^{LR} mice, in two cell models of disease, and in muscle biopsies from two DM1 patient cohorts (Figure 6A; Table S2). In these experiments, we found robust upregulation of miR-218 in muscle tissue from the HSA^{LR} mouse model. Overexpression was also conspicuous in transdifferentiated (immortalized and non-transformed) myotubes, except for cells from the patient with the lowest amount of CTG repeats in blood, and in human adult muscle biopsies. Also evident from these results was the greater dispersion of miR-218 expression values in DM1 samples from disease models and patients, perhaps reflecting the underlying phenomenon of somatic instability of CTG repeat expansions. Indeed, we detected a positive correlation between the size of CTG repeat expansion (measured in the blood) and the degree of miR-218 overexpression (Pearson correlation coefficient $r^2 = 0.556$) in deltoid muscles (Figure 6B) in the Valencia patient cohort. Indeed, receiver operating curve (ROC) analysis revealed an area under the curve (AUC) of 83%, indicating a good predictive capacity of miR-218 levels detected in muscle samples (Figure S8). Not all miR-218 expression results could be combined in these analyses because of the completely different methods used to estimate CTG repeat expansion in the two cohorts. No significant correlation was found between the age or sex of the patient and miR-218 levels (Figure S7). Thus, therapeutic targeting of miR-218 is unlikely to generate loss-of-function phenotypes.

AntagomiR-218 rescues defective cell fusion and up to 34% of transcriptome changes in the DM1 cell model

Having characterized the behavior of antagomiR-218 in HSA^{LR} model mice, we next sought a more thorough understanding of its ability to rescue cell and molecular defects in the context of disease. Patient-derived cells have characteristically low fusion capacity and myogenic differentiation delay.[42] To evaluate whether antagomiR-218 was capable of rescuing these phenotypes in myotubes, we tested the molecule at concentrations ranging from 1 to 1,000 nM (Figure 6C; Figure S9) and stained cells with Desmin, a muscle-specific type III intermediate filament essential for proper muscular structure and function.[43] The fusion index was defined as the percentage of nuclei within myotubes out of the total number of nuclei in the experimental sample. These experiments revealed significant rescue of the fusion capacity of these cells at 200 nM (38%) and a robust increase in the percentage of Desmin-positive cells in a broad range of antagomiR-218 concentrations (10–500 nM). This indicates that although the amount of cell fusion was not sufficient for significant rescue at low concentrations, muscle differentiation was already significantly enhanced by antagomiR-218 even at the lowest concentration tested.

Our next task was a comprehensive description of the transcriptome alterations brought about by the antagomiR-218 in a disease context (Figure 7). To this end, DM1 cells were transfected with

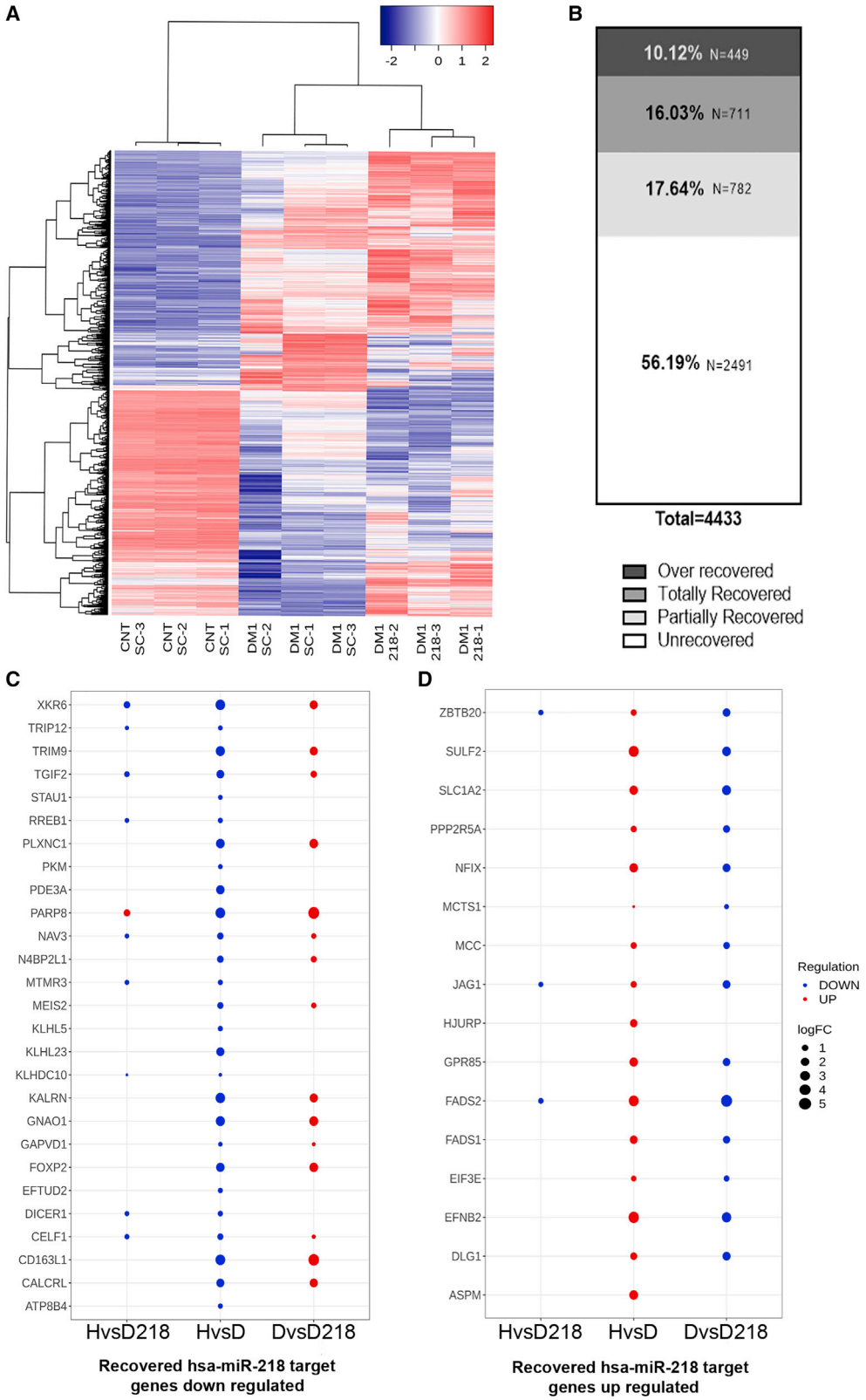

(legend on next page)

200 nM antagomiR-218, as the optimal concentration for cell fusion and mis-splicing rescue.[19] DM1 and control cells were also transfected with SC at the same concentration as control of the experimental procedure. Total RNA was extracted from the cells 4 days after treatment and processed to generate the libraries required for Illumina sequencing. After quality control, data generated included >30 million reads from each condition, which allowed transcriptome-wide analysis of gene expression changes (Table S3). As a first approach, we generated a heatmap (Figure 7A) representing the differences in transcript abundance from the median of all gene expression data and grouping the samples with the lowest differences, as shown with the dendrogram. Gene expression in the antagomiR-218-treated sample showed a trend toward overexpression (predominance of red over blue color), which is consistent with the "de-repressive" effect of antagomiRs in gene expression. Next, expression of disease-related genes (those differentially expressed in normal versus DM1 myotubes, totaling 4,433) was analyzed in antagomiR-218-treated DM1 cells and classified into four categories (Figure 7B): (1) genes that did not significantly change upon treatment, (2) genes that partially recovered normal expression, i.e., a percentage of recovery of normal expression between 10% and 50%, (3) genes that fully recovered normal expression (between 50% and 150%), and (4) genes that became over-rescued (expression above or below 150% of normal). A functional annotation was performed using fully recovered genes in Gene Ontology and Reactome databases (Table S4). By adding up partially and totally recovered genes, 33.67% of genes significantly approached a normal pattern, although this percentage may underestimate the desirable molecular effects in this cell model because it excludes MBNL1 and MBNL2 enhancement and GSK3 reduction, which were classified as over-rescued because expression changes were higher than 150% over normal values. Next, we focused on the percentage of miR-218 target transcripts that recovered normal expression upon antagomiR treatment (Figures 7C and 7D). This revealed 27 genes downregulated in disease condition, which antagomiR-218 raised to between 50% and 150% of normal expression values, and 16 upregulated genes that antagomiR rescued to close to normal levels. The greater representation of downregulated than upregulated miR-218 target transcripts in DM1 cells was consistent with our observation that miRNA was overexpressed in DM1 samples. Among the genes recovered was *Staufen1* (*Stau1*), shown to be an atrophy-associated gene contributing to progressive muscle wasting if overexpressed,[44] which remained within normal limits upon experimental treatment.

Several critical disease-related genes improve expression in response to antagomiR-218

In addition to rescuing a significant percentage of transcriptome changes detected in DM1 cells, we report an improvement in a number of critical genes in DM1 pathology at the transcript level. We centered particularly on detailed data analysis of the *MBNL1–3* family of genes, *CELF1* and *hnRNPA1* as antagonists of MBNL1 function, *DMPK* expression, and *GSK3beta* and *PRKCA*, encoding for the protein kinase C alpha, as proposed molecular mechanisms to explain increased CELF1 levels in skeletal muscles from DM1 patients[45–47] (Figure 8). *MBNL1* and *MBNL2* transcripts were significantly upregulated by antagomiR-218 in the RNA sequencing (RNA-seq) data, whereas *MBNL3* conversely showed reduced expression (Figures 8A–8C). Indeed, *MBNL3* was overexpressed in DM1 cells compared with control cells, and antagomiR-218 brought levels back to normal. This is important because in contrast to MBNL1 and 2, which are generally considered partially redundant myogenesis activators, MBNL3 has been reported as a repressor of the myogenic process.[48] *hnRNPA1* and *CELF1* (a direct miR-218 target transcript according to TargetScan database[49]) were upregulated and downregulated, respectively, in DM1 compared with healthy control cells (Figures 8D and 8E). However, in both cases their mRNA amounts approached normal levels, either completely in *hnRNPA1* (non-significant differences compared with normal control) or partially in *CELF1*, whose levels were still significantly lower in antagomiR-treated cells. Amounts of *DMPK* transcripts, which include CUG repeat expansion, were significantly downregulated in the DM1 cell model, but, more importantly, downregulation was even higher in antagomiR-218-treated patient myotubes (Figure 8F; Figures S10A–S10C). Muscle sodium channel *SCN4A* transcripts were reduced in DM1 cells and upon antagomiR-218 treatment (Figure S10D). *GSK3beta,* encoding the target of Tideglusib activity and regulated by miR-218 according to the miRTarBase database,[50] is currently being tested in congenital myotonic dystrophy patients,[51] and PKCalpha is reportedly activated in DM1 muscle samples.[47,52] In our dataset, *GSK3beta* transcription was slightly reduced and no difference was found between healthy and diseased cells in the amount of *PRKCA* transcripts, but antagomiR-218 significantly reduced the amounts of both (Figures 8G and 8H).

DISCUSSION

DM1 can be regarded, at least in part, as an MBNL1 loss-of-function disease,[5,6,13,15,16,19,22] but, unlike in most genetic disorders, the encoding gene remains perfectly normal. This opens up the possibility of using drugs to enhance its endogenous expression to compensate for pathogenic alterations caused by its sequestration by toxic *DMPK*

Figure 7. Analysis of myotube transcriptome changes brought about by antagomiR-218

(A) Heat-map of the 16,173 genes found expressed in our dataset of healthy (CNT) or DM1 cells treated with SC negative control or with antagomiR-218 (numbers refer to biological replicates) compared with the median expression of all genes in all conditions used as a reference. Differences were assigned a color according to the scale (red = overexpressed; blue = underexpressed). (B) Percentage of genes differentially expressed in CNT versus DM1 cells (disease-related genes), whose expression did not significantly approach that in normal cells (unrecovered), partially recovered (rescue between 10% and 50% of normal expression), totally recovered (between 50% and 150% of normal expression), or departed >150% from normal values (over recovered). (C and D) Totally recovered miR-218 target transcripts that antagomiR-218 manages to activate (C) or repress (D). The size of each dot represents the $\log_2$ fold change of the expression of the indicated gene for the comparisons shown: SC-treated healthy versus DM1 cells (HvsD), SC versus antagomiR-218-treated DM1 cells (DvsD218), SC-treated healthy versus antagomiR-218-treated DM1 cells (HvsD218).

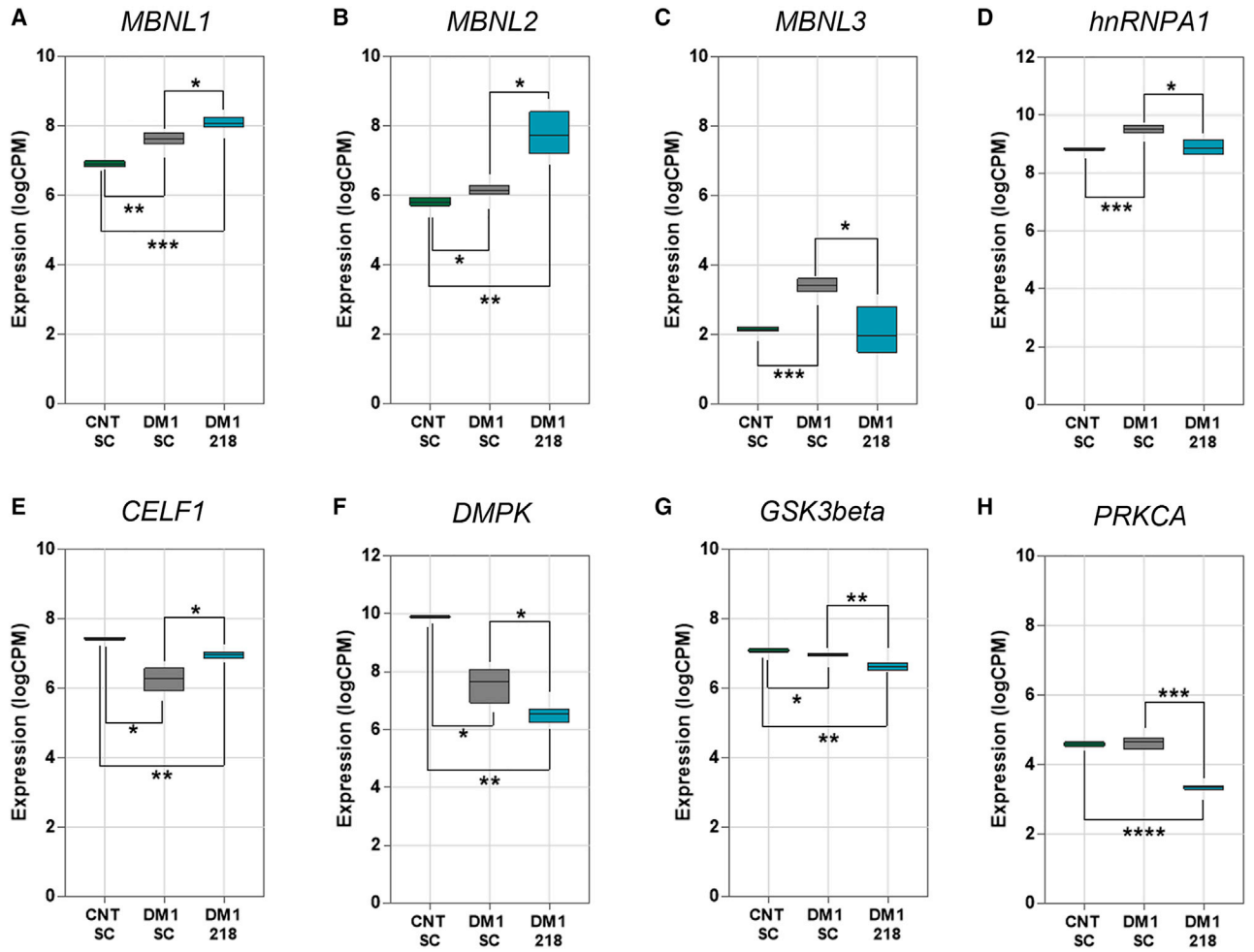

Figure 8. Critical gene expression alterations rescued by antagomiR-218

(A–H) Boxplot representation of $\log_2$ of reads per million of the indicated genes in healthy control (CNT) and DM1 cells treated with the scramble antagomiR (SC) or antagomiR-218 (218). The line marks the mean and the box the upper and lower values of the standard error from the mean. Means were compared with a Student's t test. *$p < 0.05$, **$p < 0.01$, ***$p < 0.001$.

transcripts. Here, we have explored the use of antagomiRs to block miR-218 activity as a method to enhance MBNL1 expression. Using HSA^{LR} mice, we compared response in intravenous versus subcutaneous injection, response to three doses, and activity duration from one single subcutaneous shot, which all showed behavior similar to antagomiR-23b in DM1 mice.[37] In a DM1 cell model, antagomiR-218 rescued the cell fusion index and up to 34% of transcriptome changes occurring in DM1 myotubes. Importantly, endogenous autoregulatory feedback loops should prevent any potential deleterious overexpression effects, since excess MBNL1 has been reported to induce the skipping of exon 1, leading to a protein unable to bind to RNA targets because of lacking a first complete pair of zinc fingers.[53] Notably, although MBNL1 is generally accepted to be a prime therapeutic target for DM1, the precise level of activation required to achieve a biologically meaningful effect will only be determined when MBNL1 promoting drugs are tested in patients.

One remarkable finding of the study was that *DMPK* transcripts were strongly downregulated by antagomiR-218, thus achieving the goal of reducing the root cause of DM1 symptoms: toxic RNA. *DMPK* levels in treated DM1 cells were ~41% of DM1 controls, whereas compared with healthy myotubes *DMPK* expression in antagomiR-218 treated cells was ~9.3%. This dramatic reduction in treated DM1 cells was noteworthy because ISIS 486178, a gapmer specifically targeting human *DMPK* sequences, reduced *DMPK* expression in DM1 cells to a similar percentage (~40% of normal) but at more than double the concentration of antagomiR-218 used in our study (555 nM; cf. Figure 1C in Pandey et al.[4]). A potential explanation for why antagomiR-218 reduces *DMPK* levels is that extra MBNL1 interacts with additional *DMPK* transcripts carrying CUG expansions and precipitates into extraction-resistant RNA. However, this possibility seems implausible given that no increase is observed in the number of foci in human cells[19] or in HSA^{LR} skeletal muscles (Figure 6).

Direct interaction between antagomiR-218 and CUG repeats or *DMPK* sequences is also unlikely because of a lack of significant sequence complementarity (the longest stretch identity is 7 nt). As a more indirect explanation, Tideglusib (a GSK3beta inhibitor) and sodium channel blockers have been reported to reduce mutant RNA[51] and *DMPK* mRNA and protein levels,[54] respectively, through unknown mechanisms. Interestingly, muscle sodium channel *SCN4A* transcripts were reduced in DM1 cells and antagomiR-218 treated myotubes compared with healthy controls, thus potentially contributing to *DMPK* downregulation (Figure S10D). CDK12 inhibitors are also capable of lowering *DMPK* transcript levels, but in HSA^{LR} mice this was shown to reduce the transcription of the transgene itself,[55] which was not detected in our study.

Also striking was that miR-218 was overexpressed in DM1 disease models and human muscle biopsies and that the degree of overexpression positively correlated with the size of the repeat expansions in a comparable subset of muscle biopsies. Importantly, our results are consistent with previous miRNome profiling, which found upregulated miR-218 in primary differentiated muscle cells isolated from DM1 patients.[26] Besides mature muscle, antagomiR-218 could have activity in satellite cells and therefore also influence muscle regeneration processes. In this regard, we note that a recent paper shows that DM1 skeletal muscle satellite cell (SSC) lines and primary SSCs showed decreased MBNL1 expression and elevated autophagy levels. In contrast, after MBNL1 overexpression, the proliferative capability of DM1 SSCs and phosphorylated mammalian target of rapamycin (mTOR) levels were enhanced and the autophagy levels decreased.[23] Thus, antagomiR-218 mediated upregulation of MBNL1 is anticipated to affect DM1 SSC cells positively, but this can not be directly tested in HSA^{LR} mice because CTG expansions are under the control of the skeletal actin promoter, which is not expected to be active in murine SSCs.

Oligonucleotide concentration was quantified in six tissues of HSA^{LR} mice by a custom ELISA (Figure 5A). Two weeks after systemic administration of antagomiR-218, concentrations in the brain were in the low picomolar range, confirming the low penetration of this compound across the blood-brain barrier. However, concentration was higher in muscle and in cardiac tissue, where it is especially relevant in DM1, as cardiac-conduction defects are the most common cause of death in patients. miR-218 is expressed in motor neurons,[56] which raises the possibility that a reduction in miR-218 levels might be deleterious. However, even at the highest dose of 40 mg/kg, we did not detect overt motor dysfunction in *in vivo* experiments, indicating that motor neurons were not grossly impacted by the antagomiR, at least in the conditions tested. Furthermore, motor neuron soma are located within the CNS and oligonucleotides do not readily cross the blood-brain barrier[38], although we detect minute amounts of antagomiR-218 in the brain by ELISA (Figure 5A). To explain the increase in MBNL1 levels in brain tissue in the absence of significant amounts of antagomiR, we suggest potential non-autonomous effects mediated by myokines or energy metabolism regulators, among other possibilities. For example, improvements in peripheral SMN provide long-term rescue of a severe spinal muscular atrophy mouse model at the CNS level, thus illustrating non-autonomous effects at the brain level.[57,58]

As miR-218 is characteristically overexpressed in DM1, strategies aiming at blocking miR-218 to boost MBNL1 are unlikely to encounter the potential drawback of lowering the miRNA to levels that might generate loss-of-function phenotypes. This is important because miR-218 has been described as a tumor suppressor miRNA; strongly and chronically reduced miR-218 levels therefore have the intrinsic danger of inducing tumorigenesis.[59,60] In cardiac myxoma, the most common type of human heart tumor, miR-218 was downregulated and tumorigenesis was found to depend on overexpression of myocyte enhancer factor 2D (MEF2D), which is a direct target of miR-218 repressive activity.[59] From a more general perspective, miR-218 was found to mediate tumorigenesis and metastasis, acting as a tumor suppressor gene by targeting many oncogenes related to proliferation, apoptosis, and invasion.[60] Additionally, miR-218 has been implicated as an inhibitor of osteoclast differentiation, which plays a role in osteoporosis development.[61]

Overall, the data presented here support both upregulation of endogenous levels of MBNL1 as a general therapeutic approach to treat DM1 and the use of oligonucleotide molecules to block specific repressive miRNAs. AntagomiR-218, or its chemical modifications, should now progress to pharmacokinetics and pharmacodynamic studies in its path toward early human trials.

MATERIALS AND METHODS

DM1 patients and skeletal muscle biopsies

All muscle biopsies were taken after informed consent from patients. Muscle biopsies used for miR-218 level assessment were from Donostia University Hospital (San Sebastian, Spain; previously reported in Fernandez-Costa et al.[62]) and La Fe University Hospital (Valencia, Spain; research ethics committee authorization 2014/0799). Methods for measuring the size of the CTG repeat expansion were as reported in Fernandez-Costa et al.[62]

Oligonucleotides

AntagomiR-218, agomiR-218, and the respective scramble controls were synthesized by Creative Biogene (Shirley, NY, USA) and Biomers (Germany), respectively. Sequences were as follows (m represents 2′-*O*-methyl-modified phosphoramidites, * represents phosphorothioate linkages, and chol represents cholesterol groups).

AntagomiR-218

5′-mA*mC*mAmUmGmGmUmUmAmGmAmUmCmAmAmGmCmA*mC*mA*mA*-3′-chol

Scramble control (SC)

5′-mC*mA*mGmUmAmCmUmUmUmUmGmGmUmGmUmA*mC*mA*mA*-3′-chol

Creative Biogene also synthesized the same version of AntagomiR-218 labeled with Cy3.

AgomiR-218

5′-UUGUGCUUGAUCUAACCAUGU-3′ (sense strand)

5′-mA*mC*mAmUmGmGmUmUmAmGmAmUmCmAmAmGm CmA*mC*mA*mA*-3′-chol (antisense strand)

AgomiR-Scramble

5′-UUCUCCGAACGUGUCACGUUU-3′ (sense strand)

5′-mA*mC*mGmUmGmAmCmAmCmGmUmUmCmGmGmAm GmA*mA*mU*mU*-3′-chol (antisense strand)

DM1 model mice and antagomiR administration

Experimental procedures on laboratory animals were in accordance with European law (2003/65/CE) and were approved by *Consejeria de Agricultura* of the *Generalidad Valenciana* (reference numbers 2016/VSC/PEA/0015, A1529567788818, and A1458832800370). Male transgenic HSA^{LR} mice (line 20b; homozygous)[14] were used as DM1 disease models and were compared to mice with the same genetic background (FVB) as controls. Sequences of antagomiR-218 and the Scramble control and subcutaneous injection procedures were as previously described.[19] Intravenous injections were as described in Cerro-Herreros et al.[37] PBS-injected HSA^{LR} control mice for the 12.5 mg/kg treatment were the same as reported in Cerro-Herreros et al.,[19] and PBS controls for the 3 mg/kg and 40 mg/kg treatment concentrations were also reported in Cerro-Herreros et al.[37] The last set of PBS-injected HSA^{LR} control mice were included because the animals used for this part of the study were 1 month older than those injected at 12.5 mg/kg. The overall age of mice used thus ranged from 4.5 to 5.5 months. The oligonucleotide drugs were provided by Creative Biogene (Shirley, NY, USA). Cy3-labeled antagomiR was administered in a single subcutaneous injection of 10 mg/kg in one mouse.

Cell culture conditions and cell fusion determination

Immortalized MyoD-inducible (doxycycline) DM1 and control fibroblasts are reported in Arandel et al.,[42] and additional non-transformed DM1 and control fibroblasts containing a lentivirus construct that expresses MyoD are described in Bargiela et al.[18] Cell culture conditions and handling were as reported in Cerro-Herreros et al.[19] Transdifferentiation into myotubes was induced at day 0, and test compounds were added to the cell medium at the appropriate concentration by lipofection with X-tremeGENE HP (Roche); these were replaced with fresh differentiation medium 4 h afterward. Differentiated cells were collected on day 4 and processed for RNA extraction and qRT-PCR as described below. Cell fusion quantification was as described in Sabater-Arcis et al.[63] Cells were fixed and stained with Desmin on day 4 after induction of differentiation while antagomiR treatment was as above.

RNA extraction, semiquantitative reverse transcriptase PCR (RT-PCR), and qRT-PCR

These methods were recently described in detail.[37] Briefly, total RNA from muscle samples was isolated with the miRNeasy Mini Kit (-QIAGEN; Valencia, CA, USA). 1 μg of RNA was digested with DNase I (Invitrogen) and was reverse-transcribed with SuperScript II (Invitrogen). 2 μL of cDNA was used for subsequent PCR reactions with GoTaq Polymerase (Promega) and specific primer pairs to detect alternative splicing of *Nfix* and *Clcn1* in mouse samples. *Gapdh* was amplified from 1 μL of cDNA and used as the endogenous control. PCR amplicons were quantified with ImageJ software (NIH). The percentage splice recovery (PSR) was defined as %EI minus X%DEI divided by X%DEI minus X%HEI (where EI is exon inclusion of each sample, DEI is disease exon inclusion, and HEI is healthy exon inclusion).[37] The primer sequences and exons analyzed are available in Cerro-Herreros et al.[19] In the case of RNA isolated with Hot TRIzol from cells, the protocol carried out was as described in Gagnon et al.[64] 4 μL of mouse tissue or cells cDNA at a dilution of 1/50 was used as a template for multiplex qRT-PCR with the HOT FIREPol Probe Universal qPCR Mix. The commercial TaqMan mouse probes (QIAGEN) employed were *Mbnl1* (FAM-labeled probes) and reference *Gapdh* (MAX-labeled probes). The primers and probe (IDT) for *DMPK* analysis were forward primer 5′-AGCC TGAGCCGGGAGATG-3′, reverse primer 5′-GCGTAGTTGACTG GCGAAGTT-3′, and probe 5′- AGGCCATCCGCACGGACAA CC-3′ (FAM-labeled probe). Levels of HSA transgene expression were determined by qRT-PCR according to Wheeler et al.[65] miRNA expression was quantified with specific miRCURY-locked nucleic acid miRNA PCR primers (Exiqon) according to the manufacturer. miRNA expression was normalized to endogenous U1 and U6 small nuclear RNAs (snRNAs). RNA level was assessed with an Applied Biosystems QuantStudio 5 Real-Time PCR System, and expressions relative to the endogenous references and control groups were calculated with the delta-delta Ct method ($2^{-\Delta\Delta Ct}$) method.[66]

ELISA determinations and western blotting

Quantification of Mbnl1 protein levels by ELISA and western blotting was as described in Cerro-Herreros et al.[37] Briefly, western blotting used pooled protein extracts from samples from the same experimental conditions. 20 μg of the sample was heat-denatured and electrophoresed on 12% SDS-PAGE gels. After transfer and blocking, nitrocellulose membranes were incubated with primary mouse anti-MB1a antibody (1:200, 4A8, Developmental Studies Hybridoma Bank[67]). The blot was detected with horseradish peroxidase (HRP)-conjugated anti-mouse IgG secondary antibody (1:3,500, Sigma-Aldrich) and revealed with an enhanced chemiluminescence Western Blotting Substrate (Pierce). As loading control for the cytoplasmic protein fraction in mouse samples, we used an anti-GAPDH antibody (1:3500, clone G-9, Santa Cruz) followed by an HRP-conjugated anti-mouse IgG secondary antibody (1:5,000, Sigma-Aldrich). Loading control for the nuclear protein fraction was rabbit anti-histone H3 (O/N, Millipore, 05-928, 1:1,000) followed by incubation with a secondary HRP-conjugated anti-rabbit IgG antibody (1 h, 1:3,500, Sigma-Aldrich). Images were acquired with ImageQuant LAS 4000

(GE Healthcare). Quantification was performed with ImageJ software (NIH).

Custom ELISA-based measurements of oligonucleotide concentrations in tissues were performed as described previously[68] with phosphorothioate probes (Sequence (5′ → 3′) [DIG]T*T*G*T*G*C*T*TG ATCTA*A*C*C*A*T*G*T[BIO]) double-labeled with digoxigenin and biotin. This probe was used to detect the oligonucleotide used in this study (antagomiR-218) in six different tissues (brain, kidney, liver, heart, gastrocnemius, and quadriceps) from treated HSA^{LR} mice.

Histology methods

In situ detection of CUG repeats and Mbnl1 immunofluorescence were performed with 10-μm frozen sections of the quadriceps muscles as described previously.[39] For *in situ* hybridization, the Cy3-$(CAG)_7$-Cy3-labeled probe was diluted 1:200 in the hybridization buffer. After posthybridization washes, muscle sections were incubated with fluorescein isothiocyanate (FITC)-labeled wheat germ agglutinin diluted 1:600 to stain cell membranes and mounted with DAPI mounting media (Vector). Nuclei containing at least one foci and the total number of nuclei were scored to obtain the percentage of myonuclei with foci. For Mbnl1 immunodetection, sections were incubated with mouse anti-MBNL1 antibody (1:200 clone MB1a, Wolfson Centre for Inherited Neuromuscular Disease) and detected with a FITC-labeled goat anti-mouse IgG at 1:200, and sections were mounted with DAPI mounting media (Vector). For fluorescence *in situ* hybridization (FISH) and immunofluorescence results, at least eight images per mouse were taken at 400× magnification with an LSM 800 confocal microscope (Zeiss, Jena, Germany). The Mbnl1 fluorescent signal was quantified in the confocal images by dividing the green channel intensity by the muscle area with the ImageJ software.

Cy3 moiety was synthetically attached to the 5′ end of the oligonucleotide to allow visualization of compound distribution. Cy3-labeled antagomiR was directly detectable under the fluorescence microscope in liver and kidney tissues in 10-μm frozen sections. Images from mouse tissues with Cy3-antagomiR were obtained with a Leica DM4000 B LED fluorescence microscope. In all cases, images were taken at 400× magnification.

Myotonia grade determination

Electromyographic determination of myotonia was performed with animals identified by a code to eliminate experimental bias. Animals under general anesthesia underwent a previously described procedure.[15] In brief, five electrode insertions were performed in each quadriceps muscle of both hindlimbs, and myotonic discharges were graded on a five-point scale as follows: 0, no myotonia; 1, occasional myotonic discharge in $\leq$50% of the needle insertions; 2, myotonic discharge in >50% of the insertions; 3, myotonic discharge in nearly all insertions; and 4, myotonic discharge in all insertions.

Forelimb grip strength test

Grip strength of forelimbs was measured with a Grip Strength Meter (BIO-GS3; BIOSEB, USA), following the procedures described in Cerro-Herreros et al.[37] Three consecutive measurements were performed at 30-s intervals. Body weight was acquired in parallel, and the experiment was performed blindly to eliminate bias. Raw strength data were normalized to weight and transformed to the percentage of normal force (PNF, i.e., the proximity between weight-normalized strength values of treated HSA^{LR} mice and FVB controls) as previously described.[37]

Blood assays

At 4, 15, 30, and 45 days post injection, animals were sacrificed and blood was collected with K3-EDTA (Sarstedt) by cardiac puncture exsanguination. The samples were processed by Laboratorios Montoro Botella (Valencia, Spain). White blood cell differential count (monocytes, stab cells, segmented cells, basophils, eosinophils, and lymphocytes) was measured with the Hematology Cell Counter ADVIA 120 (Siemens). The biochemistry profile of the different mouse sera (creatinine, urea, amylase, alkaline phosphatase, alanine aminotransferase [ALT], bilirubin, lipase, and bile acids) was analyzed with the cobas 600 CCE modular analyzer (Roche).

miRNA target gene luciferase reporter constructs

Procedures were as described in Cerro-Herreros et al.[19] C2C12 cells were seeded in 24-well plates. Luciferase sensor constructs containing the *Mbnl1* 3′ UTR were cloned in *pEZX-MT05-Gluc* vectors (GeneCopoeia). The constructs contained either wild-type, deletion, or PM *Mbnl1* 3′ UTRs (information contained in Method S1). Deletions lacked the seed region of miR-218, whereas PM was mutated to be an exact match of miR-218. Cells were transfected with 500 ng of miR-218 vector and 500 ng of wild-type, deletion, or PM reporter constructs. A no-miRNA control *pVmiR* was also transfected, containing an empty vector. 48 h after transfection, Gaussia luciferase (Gluc) and secreted alkaline phosphatase (SEAP) signals were read from the supernatant. Predicted miR-218 binding sites on the *Mbnl1* 3′ UTR were found through miRDB, Target Scan, and microRNA.org. The statistical differences were estimated by a Student's t test ($p < 0.05$) on normalized data.

The HeLa cells were seeded in 24-well plates at ~80% confluence and transfected with luciferase sensor constructs containing the *MBNL1* 3′ UTR cloned in the *pEZX-MT05-Gluc* vector (GeneCopoeia). HeLa cells were transfected with 200 nM of the agomiR-218 or agomiR-SC and 500 ng of the reporter construct. As a positive control, we cotransfected the agomiR-218 with a preexisting luciferase sensor construct containing the *MBNL2* 3′ UTR with a miR-218 perfect-match modification (PM-MBNL2[19]). 72 h after transfection, the supernatant was collected, and a reporter activity assay was performed. Predictions of miRNA binding to *MBNL1* 3′ UTR were obtained from the miRecords database.[35] The statistical differences were estimated by a Student's t test ($p < 0.05$) on normalized data.

RNA-seq and data analysis

Libraries were prepared with the TruSeq Stranded mRNA Library preparation kit following Illumina protocols and were sequenced with paired-end NextSeq 550. Around 30 million reads were obtained

from each sample. A quality check eliminated any read with a q value <30, using TrimGalore! (version 0.6.4_dev) (Trim Galore, RRID:SCR_011847) software. All accepted reads were aligned to genome version GRCh38.p12 with STAR software (version 2.7.3a).[69] Next, BAM results were analyzed with RSEM (version v1.3.2)[70] software to obtain gene counts. R package edgeR (version 3.28.1)[71] was used to perform a differential gene expression (DGE) test. The threshold for DGE call was an adjusted p value < 0.05.

Gene expression recovery (i.e., genes that approached a normal expression pattern) was performed for all disease-related genes (DRGs) with the following formula:

$$\%Recovery = \frac{mean\ treated\ gene\ counts - mean\ disease\ gene\ counts}{mean\ control\ gene\ counts - mean\ disease\ gene\ counts}$$

Functional annotations

R package clusterProfiler (version 3.14.3)[72] was used to perform the functional annotation for the different gene groups described. For each group, we considered the parameters of q value < 0.05 and the parameters described as necessary for each test in the package. The miRWalk (updated Mar 2020[73]) database was used to select all possible gene targets for each miRNA. Each entry with a validated interaction in miRTarBase,[50], miRDB,[74] and TargetScan was filtered. All comparisons were performed with in-house custom-made R scripts. RNA-seq data are publicly available with accession number GSE158216 in the Gene Expression Omnibus (GEO) repository.

Statistical analyses

For comparisons, mean values of molecular and functional quantitative parameters were assumed to follow normal distribution so samples could be compared with two-tailed Student t test ($\alpha = 0.05$) and Welch's correction when necessary. Statistical significance was set to $p < 0.05$. GraphPad Prism 6 software was used for statistical analyses and graphical output of data. The sample size (n) is provided in each figure. Table S5 includes the raw data of individual qRT-PCR, ELISA, myotonia grade, force, alternative exon inclusion, biodistribution of the oligonucleotide, Mbnl1 immunofluorescence intensities, and percentage of foci measurements from the indicated mouse muscles. Statistical analyses of the average values of complete blood counts and serum biochemistry profiles were performed as previously described.[37]

SUPPLEMENTAL INFORMATION

Supplemental information can be found online at https://doi.org/10.1016/j.omtn.2021.07.017.

ACKNOWLEDGMENTS

This work was funded by research grants from Instituto de Salud Carlos III, including funds from FEDER, to M.P.-A. and B.L. (PI17/00352) and HR17-00268 (TATAMI project) from the "la Caixa" Banking Foundation to R.A. I.G.-M. was funded by the Precipita Project titled "*Desarrollo de una terapia innovadora contra la distrofia miotónica*," E.C.-H. and J.M.F.-C. were supported by the postdoctoral fellowships APOSTD/2019/142 and APOSTD/2017/088 from the Fondo Social Europeo for science and investigation, while J.E.-E. was the recipient of a Santiago Grisolia fellowship (Grisolip2018/098) from the Generalidad Valenciana. Part of the equipment employed in this work has been funded by Generalitat Valenciana and co-financed with ERDF funds (OP ERDF of Comunitat Valenciana 2014-2020). Antibody MB1a (4A8) was provided by MDA Monoclonal Antibody Resources. The authors give special thanks to Juan A. Carbonell from the Incliva Bioinformatics and Biostatistics unit for his support in statistical data analysis, Prof. Guillermo Ayala from the University of Valencia for his support in statistical analyses of RNA-seq data, and Inmaculada Noguera for veterinary assistance in the University of Valencia SCSIE animal facility.

AUTHOR CONTRIBUTIONS

E.C.-H.: project administration, formal analysis, investigation, methodology, validation, visualization; I.G.-M.: formal analysis, investigation, methodology; N.M.: investigation, methodology; J.M.F.-C.: investigation, validation; A.C.-R.: investigation; S.J.O.: investigation; D.S.-M.: investigation; M.A.V.: project administration, conceptualization; M.J.W.: funding acquisition; J.P.-G.: resources; J.J.V.: resources; A.L.M.: resources; J.E.-E.: software, formal analysis; M.P.-A.: conceptualization, funding acquisition; B.L.: project administration; R.A.: conceptualization, funding acquisition, resources, supervision, writing.

DECLARATION OF INTERESTS

B.L., R.A., J.M.F.-C., and E.C.-H. are inventors in patent PCT/EP2017/073685. This patent is currently licensed to Arthex Biotech, of which B.L. and R.A. are founders and CEO and scientific consultant, respectively. B.L. and R.A. each hold more than 5% ownership of Arthex, a company with related interests.

REFERENCES

1. Miller, J.W., Urbinati, C.R., Teng-Umnuay, P., Stenberg, M.G., Byrne, B.J., Thornton, C.A., and Swanson, M.S. (2000). Recruitment of human muscleblind proteins to (CUG)(n) expansions associated with myotonic dystrophy. EMBO J. *19*, 4439–4448.

2. Fardaei, M., Larkin, K., Brook, J.D., and Hamshere, M.G. (2001). In vivo co-localisation of MBNL protein with DMPK expanded-repeat transcripts. Nucleic Acids Res. *29*, 2766–2771.

3. Lee, J.E., Bennett, C.F., and Cooper, T.A. (2012). RNase H-mediated degradation of toxic RNA in myotonic dystrophy type 1. Proc. Natl. Acad. Sci. USA *109*, 4221–4226.

4. Pandey, S.K., Wheeler, T.M., Justice, S.L., Kim, A., Younis, H.S., Gattis, D., Jauvin, D., Puymirat, J., Swayze, E.E., Freier, S.M., et al. (2015). Identification and characterization of modified antisense oligonucleotides targeting DMPK in mice and nonhuman primates for the treatment of myotonic dystrophy type 1. J. Pharmacol. Exp. Ther. *355*, 329–340.

5. Zhang, F., Bodycombe, N.E., Haskell, K.M., Sun, Y.L., Wang, E.T., Morris, C.A., Jones, L.H., Wood, L.D., and Pletcher, M.T. (2017). A flow cytometry-based screen identifies MBNL1 modulators that rescue splicing defects in myotonic dystrophy type I. Hum. Mol. Genet. *26*, 3056–3068.

6. Chen, G., Masuda, A., Konishi, H., Ohkawara, B., Ito, M., Kinoshita, M., Kiyama, H., Matsuura, T., and Ohno, K. (2016). Phenylbutazone induces expression of MBNL1 and suppresses formation of MBNL1-CUG RNA foci in a mouse model of myotonic dystrophy. Sci. Rep. *6*, 25317.

7. Ashizawa, T., Gagnon, C., Groh, W.J., Gutmann, L., Johnson, N.E., Meola, G., Moxley, R., 3rd, Pandya, S., Rogers, M.T., Simpson, E., et al. (2018). Consensus-based care recommendations for adults with myotonic dystrophy type 1. Neurol. Clin. Pract. *8*, 507–520.

8. Smith, C.A., and Gutmann, L. (2016). Myotonic Dystrophy Type 1 Management and Therapeutics. Curr. Treat. Options Neurol. *18*, 52.

9. Brook, J.D., McCurrach, M.E., Harley, H.G., Buckler, A.J., Church, D., Aburatani, H., Hunter, K., Stanton, V.P., Thirion, J.P., Hudson, T., et al. (1992). Molecular basis of myotonic dystrophy: expansion of a trinucleotide (CTG) repeat at the 3′ end of a transcript encoding a protein kinase family member. Cell *69*, 385.

10. Mahadevan, M., Tsilfidis, C., Sabourin, L., Shutler, G., Amemiya, C., Jansen, G., Neville, C., Narang, M., Barceló, J., O'Hoy, K., et al. (1992). Myotonic dystrophy mutation: an unstable CTG repeat in the 3′ untranslated region of the gene. Science *255*, 1253–1255.

11. Kanadia, R.N., Johnstone, K.A., Mankodi, A., Lungu, C., Thornton, C.A., Esson, D., Timmers, A.M., Hauswirth, W.W., and Swanson, M.S. (2003). A muscleblind knockout model for myotonic dystrophy. Science *302*, 1978–1980.

12. Charizanis, K., Lee, K.-Y., Batra, R., Goodwin, M., Zhang, C., Yuan, Y., Shiue, L., Cline, M., Scotti, M.M., Xia, G., et al. (2012). Muscleblind-like 2-mediated alternative splicing in the developing brain and dysregulation in myotonic dystrophy. Neuron *75*, 437–450.

13. Lee, K.-Y., Li, M., Manchanda, M., Batra, R., Charizanis, K., Mohan, A., Warren, S.A., Chamberlain, C.M., Finn, D., Hong, H., et al. (2013). Compound loss of muscleblind-like function in myotonic dystrophy. EMBO Mol. Med. *5*, 1887–1900.

14. Mankodi, A., Logigian, E., Callahan, L., McClain, C., White, R., Henderson, D., Krym, M., and Thornton, C.A. (2000). Myotonic dystrophy in transgenic mice expressing an expanded CUG repeat. Science *289*, 1769–1773.

15. Kanadia, R.N., Shin, J., Yuan, Y., Beattie, S.G., Wheeler, T.M., Thornton, C.A., and Swanson, M.S. (2006). Reversal of RNA missplicing and myotonia after muscleblind overexpression in a mouse poly(CUG) model for myotonic dystrophy. Proc. Natl. Acad. Sci. USA *103*, 11748–11753.

16. Chamberlain, C.M., and Ranum, L.P.W. (2012). Mouse model of muscleblind-like 1 overexpression: skeletal muscle effects and therapeutic promise. Hum. Mol. Genet. *21*, 4645–4654.

17. Huang, K., Masuda, A., Chen, G., Bushra, S., Kamon, M., Araki, T., Kinoshita, M., Ohkawara, B., Ito, M., and Ohno, K. (2020). Inhibition of cyclooxygenase-1 by nonsteroidal anti-inflammatory drugs demethylates MeR2 enhancer and promotes Mbnl1 transcription in myogenic cells. Sci. Rep. *10*, 2558.

18. Bargiela, A., Sabater-Arcis, M., Espinosa-Espinosa, J., Zulaica, M., Lopez de Munain, A., and Artero, R. (2019). Increased Muscleblind levels by chloroquine treatment improve myotonic dystrophy type 1 phenotypes in in vitro and in vivo models. Proc. Natl. Acad. Sci. USA *116*, 25203–25213.

19. Cerro-Herreros, E., Sabater-Arcis, M., Fernandez-Costa, J.M., Moreno, N., Perez-Alonso, M., Llamusi, B., and Artero, R. (2018). miR-23b and miR-218 silencing increase Muscleblind-like expression and alleviate myotonic dystrophy phenotypes in mammalian models. Nat. Commun. *9*, 2482.

20. Cerro-Herreros, E., Fernandez-Costa, J.M., Sabater-Arcis, M., Llamusi, B., and Artero, R. (2016). Derepressing muscleblind expression by miRNA sponges ameliorates myotonic dystrophy-like phenotypes in Drosophila. Sci. Rep. *6*, 36230.

21. Osborne, R.J., Lin, X., Welle, S., Sobczak, K., O'Rourke, J.R., Swanson, M.S., and Thornton, C.A. (2009). Transcriptional and post-transcriptional impact of toxic RNA in myotonic dystrophy. Hum. Mol. Genet. *18*, 1471–1481.

22. Du, H., Cline, M.S., Osborne, R.J., Tuttle, D.L., Clark, T.A., Donohue, J.P., Hall, M.P., Shiue, L., Swanson, M.S., Thornton, C.A., and Ares, M., Jr. (2010). Aberrant alternative splicing and extracellular matrix gene expression in mouse models of myotonic dystrophy. Nat. Struct. Mol. Biol. *17*, 187–193.

23. Song, K.-Y., Guo, X.-M., Wang, H.-Q., Zhang, L., Huang, S.-Y., Huo, Y.-C., Zhang, G., Feng, J.-Z., Zhang, R.-R., Ma, Y., et al. (2020). MBNL1 reverses the proliferation defect of skeletal muscle satellite cells in myotonic dystrophy type 1 by inhibiting autophagy via the mTOR pathway. Cell Death Dis. *11*, 545.

24. Lin, X., Miller, J.W., Mankodi, A., Kanadia, R.N., Yuan, Y., Moxley, R.T., Swanson, M.S., and Thornton, C.A. (2006). Failure of MBNL1-dependent post-natal splicing transitions in myotonic dystrophy. Hum. Mol. Genet. *15*, 2087–2097.

25. Batra, R., Charizanis, K., Manchanda, M., Mohan, A., Li, M., Finn, D.J., Goodwin, M., Zhang, C., Sobczak, K., Thornton, C.A., and Swanson, M.S. (2014). Loss of MBNL leads to disruption of developmentally regulated alternative polyadenylation in RNA-mediated disease. Mol. Cell *56*, 311–322.

26. Rau, F., Freyermuth, F., Fugier, C., Villemin, J.-P., Fischer, M.-C., Jost, B., Dembele, D., Gourdon, G., Nicole, A., Duboc, D., et al. (2011). Misregulation of miR-1 processing is associated with heart defects in myotonic dystrophy. Nat. Struct. Mol. Biol. *18*, 840–845.

27. Masuda, A., Andersen, H.S., Doktor, T.K., Okamoto, T., Ito, M., Andresen, B.S., and Ohno, K. (2012). CUGBP1 and MBNL1 preferentially bind to 3′ UTRs and facilitate mRNA decay. Sci. Rep. *2*, 209.

28. Wang, E.T., Cody, N.A.L., Jog, S., Biancolella, M., Wang, T.T., Treacy, D.J., Luo, S., Schroth, G.P., Housman, D.E., Reddy, S., et al. (2012). Transcriptome-wide regulation of pre-mRNA splicing and mRNA localization by muscleblind proteins. Cell *150*, 710–724.

29. Adereth, Y., Dammai, V., Kose, N., Li, R., and Hsu, T. (2005). RNA-dependent integrin α3 protein localization regulated by the Muscleblind-like protein MLP1. Nat. Cell Biol. *7*, 1240–1247.

30. Wang, E.T., Ward, A.J., Cherone, J.M., Giudice, J., Wang, T.T., Treacy, D.J., Lambert, N.J., Freese, P., Saxena, T., Cooper, T.A., and Burge, C.B. (2015). Antagonistic regulation of mRNA expression and splicing by CELF and MBNL proteins. Genome Res. *25*, 858–871.

31. Li, M., Zhuang, Y., Batra, R., Thomas, J.D., Li, M., Nutter, C.A., Scotti, M.M., Carter, H.A., Wang, Z.J., Huang, X.-S., et al. (2020). HNRNPA1-induced spliceopathy in a transgenic mouse model of myotonic dystrophy. Proc. Natl. Acad. Sci. USA *117*, 5472–5477.

32. Charlet-B, N., Savkur, R.S., Singh, G., Philips, A.V., Grice, E.A., and Cooper, T.A. (2002). Loss of the muscle-specific chloride channel in type 1 myotonic dystrophy due to misregulated alternative splicing. Mol. Cell *10*, 45–53.

33. Fugier, C., Klein, A.F., Hammer, C., Vassilopoulos, S., Ivarsson, Y., Toussaint, A., Tosch, V., Vignaud, A., Ferry, A., Messaddeq, N., et al. (2011). Misregulated alternative splicing of BIN1 is associated with T tubule alterations and muscle weakness in myotonic dystrophy. Nat. Med. *17*, 720–725.

34. Wang, E.T., Treacy, D., Eichinger, K., Struck, A., Estabrook, J., Olafson, H., Wang, T.T., Bhatt, K., Westbrook, T., Sedehizadeh, S., et al. (2019). Transcriptome alterations in myotonic dystrophy skeletal muscle and heart. Hum. Mol. Genet. *28*, 1312–1321.

35. Xiao, F., Zuo, Z., Cai, G., Kang, S., Gao, X., and Li, T. (2009). miRecords: an integrated resource for microRNA-target interactions. Nucleic Acids Res. *37*, D105–D110.

36. Shen, W., De Hoyos, C.L., Migawa, M.T., Vickers, T.A., Sun, H., Low, A., Bell, T.A., 3rd, Rahdar, M., Mukhopadhyay, S., Hart, C.E., et al. (2019). Chemical modification of PS-ASO therapeutics reduces cellular protein-binding and improves the therapeutic index. Nat. Biotechnol. *37*, 640–650.

37. Cerro-Herreros, E., González-Martínez, I., Moreno-Cervera, N., Overby, S., Pérez-Alonso, M., Llamusí, B., and Artero, R. (2020). Therapeutic Potential of AntagomiR-23b for Treating Myotonic Dystrophy. Mol. Ther. Nucleic Acids *21*, 837–849.

38. Geary, R.S., Norris, D., Yu, R., and Bennett, C.F. (2015). Pharmacokinetics, biodistribution and cell uptake of antisense oligonucleotides. Adv. Drug Deliv. Rev. *87*, 46–51.

39. Bisset, D.R., Stepniak-Konieczna, E.A., Zavaljevski, M., Wei, J., Carter, G.T., Weiss, M.D., and Chamberlain, J.R. (2015). Therapeutic impact of systemic AAV-mediated RNA interference in a mouse model of myotonic dystrophy. Hum. Mol. Genet. *24*, 4971–4983.

40. Zhang, B., and Pan, X. (2009). RDX induces aberrant expression of microRNAs in mouse brain and liver. Environ. Health Perspect. *117*, 231–240.

41. Hsu, S.-D., Chu, C.-H., Tsou, A.-P., Chen, S.-J., Chen, H.-C., Hsu, P.W.-C., Wong, Y.-H., Chen, Y.-H., Chen, G.-H., and Huang, H.-D. (2008). miRNAMap 2.0: genomic maps of microRNAs in metazoan genomes. Nucleic Acids Res. *36*, D165–D169.

42. Arandel, L., Polay Espinoza, M., Matloka, M., Bazinet, A., De Dea Diniz, D., Naouar, N., Rau, F., Jollet, A., Edom-Vovard, F., Mamchaoui, K., et al. (2017). Immortalized human myotonic dystrophy muscle cell lines to assess therapeutic compounds. Dis. Model. Mech. *10*, 487–497.

43. Hnia, K., Ramspacher, C., Vermot, J., and Laporte, J. (2015). Desmin in muscle and associated diseases: beyond the structural function. Cell Tissue Res. *360*, 591–608.

44. Crawford Parks, T.E., Marcellus, K.A., Péladeau, C., Jasmin, B.J., and Ravel-Chapuis, A. (2020). Overexpression of Staufen1 in DM1 mouse skeletal muscle exacerbates dystrophic and atrophic features. Hum. Mol. Genet. *29*, 2185–2199.

45. Timchenko, N.A., Cai, Z.J., Welm, A.L., Reddy, S., Ashizawa, T., and Timchenko, L.T. (2001). RNA CUG repeats sequester CUGBP1 and alter protein levels and activity of CUGBP1. J. Biol. Chem. *276*, 7820–7826.

46. Jones, K., Wei, C., Iakova, P., Bugiardini, E., Schneider-Gold, C., Meola, G., Woodgett, J., Killian, J., Timchenko, N.A., and Timchenko, L.T. (2012). GSK3β mediates muscle pathology in myotonic dystrophy. J. Clin. Invest. *122*, 4461–4472.

47. Kuyumcu-Martinez, N.M., Wang, G.-S., and Cooper, T.A. (2007). Increased steady-state levels of CUGBP1 in myotonic dystrophy 1 are due to PKC-mediated hyperphosphorylation. Mol. Cell *28*, 68–78.

48. Lee, K.-S., Smith, K., Amieux, P.S., and Wang, E.H. (2008). MBNL3/CHCR prevents myogenic differentiation by inhibiting MyoD-dependent gene transcription. Differentiation *76*, 299–309.

49. Shin, C., Nam, J.-W., Farh, K.K.-H., Chiang, H.R., Shkumatava, A., and Bartel, D.P. (2010). Expanding the microRNA targeting code: functional sites with centered pairing. Mol. Cell *38*, 789–802.

50. Huang, H.-Y., Lin, Y.-C.-D., Li, J., Huang, K.-Y., Shrestha, S., Hong, H.-C., Tang, Y., Chen, Y.-G., Jin, C.-N., Yu, Y., et al. (2020). miRTarBase 2020: updates to the experimentally validated microRNA-target interaction database. Nucleic Acids Res. *48* (D1), D148–D154.

51. Wang, M., Weng, W.-C., Stock, L., Lindquist, D., Martinez, A., Gourdon, G., Timchenko, N., Snape, M., and Timchenko, L. (2019). Correction of Glycogen Synthase Kinase 3β in Myotonic Dystrophy 1 Reduces the Mutant RNA and Improves Postnatal Survival of DMSXL Mice. Mol. Cell. Biol. *39*, e00155-19. 31383751.

52. Wei, C., Jones, K., Timchenko, N.A., and Timchenko, L. (2013). GSK3β is a new therapeutic target for myotonic dystrophy type 1. Rare Dis. *1*, e26555.

53. Konieczny, P., Stepniak-Konieczna, E., Taylor, K., Sznajder, L.J., and Sobczak, K. (2017). Autoregulation of MBNL1 function by exon 1 exclusion from MBNL1 transcript. Nucleic Acids Res. *45*, 1760–1775.

54. Witherspoon, L., O'Reilly, S., Hadwen, J., Tasnim, N., MacKenzie, A., and Farooq, F. (2015). Sodium Channel Inhibitors Reduce DMPK mRNA and Protein. Clin. Transl. Sci. *8*, 298–304.

55. Ketley, A., Wojciechowska, M., Ghidelli-Disse, S., Bamborough, P., Ghosh, T.K., Morato, M.L., Sedehizadeh, S., Malik, N.A., Tang, Z., Powalowska, P., et al. (2020). CDK12 inhibition reduces abnormalities in cells from patients with myotonic dystrophy and in a mouse model. Sci. Transl. Med. *12*, eaaz2415.

56. Thiebes, K.P., Nam, H., Cambronne, X.A., Shen, R., Glasgow, S.M., Cho, H.-H., Kwon, J.-S., Goodman, R.H., Lee, J.W., Lee, S., and Lee, S.K. (2015). miR-218 is essential to establish motor neuron fate as a downstream effector of Isl1-Lhx3. Nat. Commun. *6*, 7718.

57. Hua, Y., Sahashi, K., Rigo, F., Hung, G., Horev, G., Bennett, C.F., and Krainer, A.R. (2011). Peripheral SMN restoration is essential for long-term rescue of a severe spinal muscular atrophy mouse model. Nature *478*, 123–126.

58. Hammond, S.M., Hazell, G., Shabanpoor, F., Saleh, A.F., Bowerman, M., Sleigh, J.N., Meijboom, K.E., Zhou, H., Muntoni, F., Talbot, K., et al. (2016). Systemic peptide-mediated oligonucleotide therapy improves long-term survival in spinal muscular atrophy. Proc. Natl. Acad. Sci. USA *113*, 10962–10967.

59. Cao, Q., Dong, P., Wang, Y., Zhang, J., Shi, X., and Wang, Y. (2015). miR-218 suppresses cardiac myxoma proliferation by targeting myocyte enhancer factor 2D. Oncol. Rep. *33*, 2606–2612.

60. Lu, Y.-F., Zhang, L., Waye, M.M.Y., Fu, W.-M., and Zhang, J.-F. (2015). MiR-218 mediates tumorigenesis and metastasis: Perspectives and implications. Exp. Cell Res. *334*, 173–182.

61. Wang, W., Yang, L., Zhang, D., Gao, C., Wu, J., Zhu, Y., and Zhang, H. (2018). MicroRNA-218 Negatively Regulates Osteoclastogenic Differentiation by Repressing the Nuclear Factor-κB Signaling Pathway and Targeting Tumor Necrosis Factor Receptor 1. Cell. Physiol. Biochem. *48*, 339–347.

62. Fernandez-Costa, J.M., Garcia-Lopez, A., Zuñiga, S., Fernandez-Pedrosa, V., Felipo-Benavent, A., Mata, M., Jaka, O., Aiastui, A., Hernandez-Torres, F., Aguado, B., et al. (2013). Expanded CTG repeats trigger miRNA alterations in Drosophila that are conserved in myotonic dystrophy type 1 patients. Hum. Mol. Genet. *22*, 704–716.

63. Sabater-Arcis, M., Bargiela, A., Furling, D., and Artero, R. (2020). miR-7 Restores Phenotypes in Myotonic Dystrophy Muscle Cells by Repressing Hyperactivated Autophagy. Mol. Ther. Nucleic Acids *19*, 278–292.

64. Gagnon, K.T., Li, L., Janowski, B.A., and Corey, D.R. (2014). Analysis of nuclear RNA interference in human cells by subcellular fractionation and Argonaute loading. Nat. Protoc. *9*, 2045–2060.

65. Wheeler, T.M., Sobczak, K., Lueck, J.D., Osborne, R.J., Lin, X., Dirksen, R.T., and Thornton, C.A. (2009). Reversal of RNA dominance by displacement of protein sequestered on triplet repeat RNA. Science *325*, 336–339.

66. Rao, X., Huang, X., Zhou, Z., and Lin, X. (2013). An improvement of the 2^(-delta delta CT) method for quantitative real-time polymerase chain reaction data analysis. Biostat. Bioinforma. Biomath. *3*, 71–85.

67. Holt, I., Mittal, S., Furling, D., Butler-Browne, G.S., Brook, J.D., and Morris, G.E. (2007). Defective mRNA in myotonic dystrophy accumulates at the periphery of nuclear splicing speckles. Genes Cells *12*, 1035–1048.

68. Burki, U., Keane, J., Blain, A., O'Donovan, L., Gait, M.J., Laval, S.H., and Straub, V. (2015). Development and Application of an Ultrasensitive Hybridization-Based ELISA Method for the Determination of Peptide-Conjugated Phosphorodiamidate Morpholino Oligonucleotides. Nucleic Acid Ther. *25*, 275–284.

69. Dobin, A., Davis, C.A., Schlesinger, F., Drenkow, J., Zaleski, C., Jha, S., Batut, P., Chaisson, M., and Gingeras, T.R. (2013). STAR: ultrafast universal RNA-seq aligner. Bioinformatics *29*, 15–21.

70. Li, B., and Dewey, C.N. (2011). RSEM: accurate transcript quantification from RNA-Seq data with or without a reference genome. BMC Bioinformatics *12*, 323.

71. Robinson, M.D., McCarthy, D.J., and Smyth, G.K. (2010). edgeR: a Bioconductor package for differential expression analysis of digital gene expression data. Bioinformatics *26*, 139–140.

72. Yu, G., Wang, L.-G., Han, Y., and He, Q.-Y. (2012). clusterProfiler: an R package for comparing biological themes among gene clusters. OMICS *16*, 284–287.

73. Sticht, C., De La Torre, C., Parveen, A., and Gretz, N. (2018). miRWalk: An online resource for prediction of microRNA binding sites. PLoS ONE *13*, e0206239.

74. Chen, Y., and Wang, X. (2020). miRDB: an online database for prediction of functional microRNA targets. Nucleic Acids Res. *48* (D1), D127–D131.